Published in final edited form as:

Cell Metab. 2020 November 03; 32(5): 751–766.e11. doi:10.1016/j.cmet.2020.10.006.

Multi-Tissue Acceleration of the Mitochondrial Phosphoenolpyruvate Cycle Improves Whole-Body Metabolic Health

Abudukadier Abulizi[1], **Rebecca L. Cardone**[1], **Romana Stark**[2], **Sophie L. Lewandowski**[3], **Xiaojian Zhao**[1], **Joelle Hillion**[1], **Lingjun Ma**[1], **Raghav Sehgal**[1], **Tiago C. Alves**[1], **Craig Thomas**[4], **Charles Kung**[5], **Bei Wang**[1], **Stephan Siebel**[1], **Zane B. Andrews**[2], **Graeme F. Mason**[6], **Jesse Rinehart**[7], **Matthew J. Merrins**[3], **Richard G. Kibbey**[1,7,8,*]

[1]Department of Internal Medicine, Yale University, New Haven, CT 06520, USA

[2]Department of Physiology, Monash University, Melbourne, VIC 3800, Australia

[3]Department of Medicine, Division of Endocrinology, Diabetes, and Metabolism, and Department of Biomolecular Chemistry, University of Wisconsin-Madison, and William S. Middleton Memorial Veterans Hospital, Madison, WI, USA

[4]Division of Preclinical Innovation, National Center for Advancing Translational Sciences, and Lymphoid Malignancies Branch, National Cancer Institute, National Institutes of Health, Bethesda, MD 20892, USA

[5]Agios Pharmaceuticals, Cambridge, MA 02139, USA

[6]Department of Diagnostic Radiology and Psychiatry, Yale University, New Haven, CT 06520, USA

[7]Department of Cellular & Molecular Physiology, Yale University, New Haven, CT 06520, USA

[8]Lead Contact

SUMMARY

The mitochondrial GTP (mtGTP)-dependent phosphoenolpyruvate (PEP) cycle couples mitochondrial PEPCK (PCK2) to pyruvate kinase (PK) in the liver and pancreatic islets to regulate glucose homeostasis. Here, small molecule PK activators accelerated the PEP cycle to improve islet function, as well as metabolic homeostasis, in preclinical rodent models of diabetes. In

*Correspondence: richard.kibbey@yale.edu.

AUTHOR CONTRIBUTIONS

R.G.K. conceived the study and wrote the paper with A.A., R.L.C., and R. Stark. A.A. and R.L.C. performed the main body of experiments with contributions from R. Stark., T.C.A., S.L.L., J.H., and L.M. and assisted by B.W., X.Z., R. Sehgal, and S.S. C.K., C.T., R.S., Z.B.A., G.F.M., and J.R. provided reagents and technical expertise. R.G.K., G.F.M., M.J.M., R.S., and Z.B.A. obtained funding. R.G.K., A.A., R.L.C., R. Stark., S.L.L., M.J.M., C.T., and C.K. interpreted the data and edited the manuscript.

SUPPLEMENTAL INFORMATION

Supplemental Information can be found online at https://doi.org/10.1016/j.cmet.2020.10.006.

DECLARATION OF INTERESTS

C.K. is an employee of and stockholder in Agios Pharmaceuticals. R.G.K. has been a paid consultant for Agios Pharmaceuticals. The remaining authors declare no competing interests.

SUPPORTING CITATIONS

The following references appear in the Supplemental Information: Anastasiou et al. (2012); Boxer et al. (2010); Jiang et al. (2010).

contrast, treatment with a PK activator did not improve insulin secretion in *pck2*$^{-/-}$ mice. Unlike other clinical secretagogues, PK activation enhanced insulin secretion but also had higher insulin content and markers of differentiation. In addition to improving insulin secretion, acute PK activation short-circuited gluconeogenesis to reduce endogenous glucose production while accelerating red blood cell glucose turnover. Four-week delivery of a PK activator *in vivo* remodeled PK phosphorylation, reduced liver fat, and improved hepatic and peripheral insulin sensitivity in HFD-fed rats. These data provide a preclinical rationale for PK activation to accelerate the PEP cycle to improve metabolic homeostasis and insulin sensitivity.

Graphical Abstract

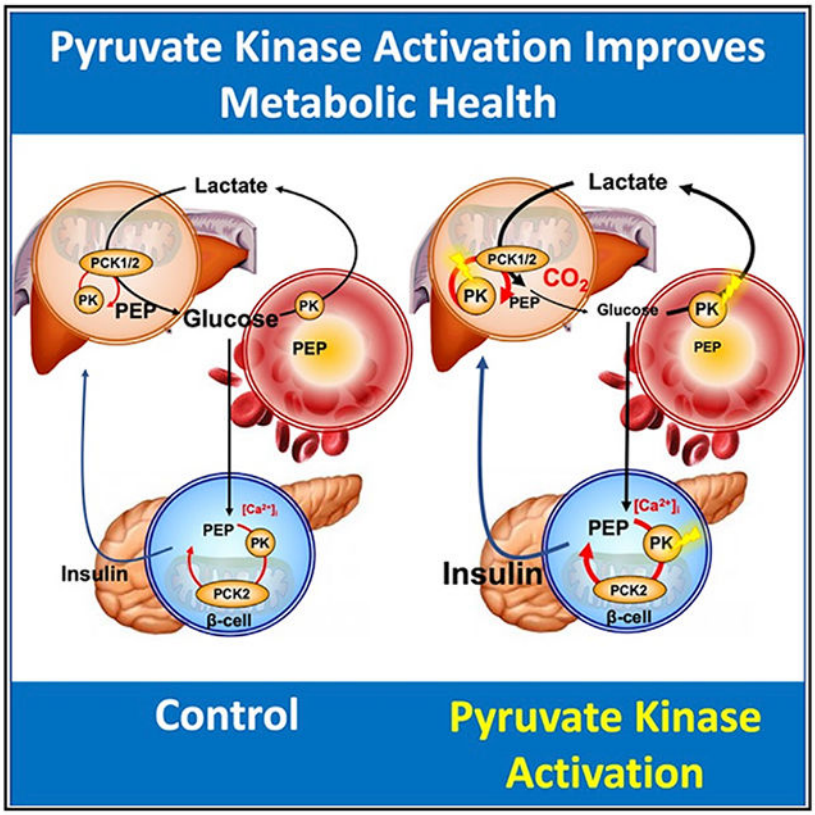

In Brief

Abulizi et al. show that small molecule activation of mitochondrial PEPCK (*pck2*)-dependent phosphoenolpyruvate (PEP) cycling amplifies glucose-stimulated insulin secretion without evidence of islet injury and improves insulin sensitivity *in vivo.* These are accompanied by decreased gluconeogenesis, increased red blood cell glycolysis, and reduced hepatic steatosis in preclinical rodent models of diabetes.

INTRODUCTION

An aspect of the current consensus model of beta cell glucose sensing is that glucokinase (GK)-determined oxidative phosphorylation (OxPhos) lowers ADP to control plasma

membrane depolarization needed for insulin secretion. Further based on the current model, pharmacological targeting of glucose entry (e.g., with GK activators, GKa) and depolarization of the beta cell membrane (e.g., with sulphonylureas, SU) stimulate insulin secretion, but such approaches have had incrementally diminished long-term therapeutic success (De Ceuninck et al., 2013; Efanova et al., 1998; Erion et al., 2014; Iwakura et al., 2000). Successful targeting of the intermediate steps in the canonical pathway by other approaches, including enhancing OxPhos, have also been of limited success, with no agents currently approved for use in humans.

The OxPhos-independent mitochondrial GTP (mtGTP)-dependent phosphoenolpyruvate (PEP) cycle is a metabolic signaling pathway important for nutrient-stimulated insulin secretion that provides a targetable therapeutic opportunity (Figure 1A) (Jesinkey et al., 2019; Kibbey et al., 2007; Lewandowski et al., 2020; Stark et al., 2009). This pathway begins with pyruvate entry into the TCA cycle (anaplerosis) via the mitochondrial enzyme pyruvate carboxylase (PC) to generate oxaloacetic acid (OAA). OAA carbons are removed from the TCA cycle (cataplerosis) as PEP following the action of mtGTP-dependent PCK2 (Alves et al., 2015; Jesinkey et al., 2019; Kibbey et al., 2007; Stark et al., 2009). The cycle is completed when the PEP is then enzymatically hydrolyzed back to pyruvate by PK in order to lower cytosolic ADP. PK-mediated ADP lowering first slows down OxPhos and then closes K_{ATP} channels to depolarize the plasma membrane (Lewandowski et al., 2020). As predicted by this new, more dynamic model of glucose-stimulated insulin secretion (GSIS), use of cell-permeable, small molecule allosteric PK activators that lower the K_m for PEP increases the frequency of metabolic and electrical oscillations within beta cells, and thus stimulates insulin release (Lewandowski et al., 2020). To further test the potential therapeutic relevance of PK activation, we asked whether accelerating the PEP cycle with intravenous or oral delivery of a PK activator (1) works *in vivo*, (2) depends on PCK2, (3) impacts islet performance without injury, and (4) enhances insulin secretion in preclinical rodent models and diabetic human islets.

But it should be noted that pharmacologic PEP cycle acceleration would not be limited to just beta cells as activatable forms of PK (PKM2, PKL, and PKR) are also found in the liver and red blood cells (RBCs). Indeed, small molecule activation of the PEP cycle in the liver would short-circuit gluconeogenesis, while hastening glucose turnover in RBCs. And here we found that use of a PK activator to accelerate the PEP cycle resulted in (1) decreased gluconeogenesis, (2) lowered tissue and circulating lipids, (3) increased peripheral glucose turnover (including RBCs), and (4) improved tissue-specific insulin sensitivity. These results suggest that use of PK activators may represent a potent new avenue in the treatment of diabetes and its complications.

RESULTS

Enhancing Oxidative Metabolism Does Not Improve Islet Function

Pyruvate dehydrogenase (PDH) kinase (PDK) phosphorylates and inhibits PDH. PDK inhibition with dichoroacetate (DCA) reduces phosphorylation of PDH and provides an acute mechanism to increase the oxidation of glucose (Sharma et al., 2019). Rather than improving GSIS by activating PDH, we confirmed prior *in vivo* and *in vitro* reports

(Akhmedov et al., 2012) that DCA reduces insulin secretion in rat islets and rat insulinoma cells (INS-1) (Figures S1A and S1B). Mice with knockout of both isoform 2 and 4 of PDK (PDKdKO) had higher glucose oxidation rates as well as improved glucose tolerance, but paradoxically at the same time had reduced plasma insulin levels (Wu et al., 2018). We thus asked whether increasing the oxidation by reducing PDK activity with PDKdKO was similar to DCA in intact islets but without the off-target effects of DCA (James et al., 2017; Jeoung et al., 2012). We found that perifused islets from *PDKdKO* mice had normal first-phase insulin secretion, but the mitochondria-dependent second phase was significantly lowered (Figure S1C).

Pck2$^{-/-}$ Mice Have Impaired Beta Cell Function *In Vivo*

As an alternative target to enhancing pyruvate oxidation, increased pyruvate anaplerosis coupled to mtGTP and PCK2-mediated PEP synthesis are linked to insulin secretion (Alves et al., 2015; Jesinkey et al., 2019; Kibbey et al., 2007; Stark et al., 2009). To evaluate the role of *Pck2 in vivo*, we generated Pck2 knockout mice and backcrossed them onto the C57BL/6J strain (Figures S1D–S1F). At 8 weeks of age, the male mice had similar body weights, plasma glucagon levels, and islet insulin content compared to wild type (WT) (Figures S1G–S1I). Fasting plasma glucose was elevated from regular chow-fed *Pck2*$^{-/-}$ mice, indicative of defective glucose homeostasis (Figure S1J). Independent of potential changes in insulin sensitivity in the whole-body knockout, beta cell function was directly tested by hyperglycemic clamp. *Pck2*$^{-/-}$ mice required a lower glucose infusion rate (GIR) to maintain glycemia at 300 mg/dL (Figures 1B and 1C) and were deficient in phasic insulin secretion (Figure 1D) compared to WT. Clamped insulin more than tripled in controls but was not significantly higher in *Pck2*$^{-/-}$ mice (Figure 1D), indicating an important role for PCK2 in sustaining GSIS *in vivo.*

Amplification of Insulin Secretion by PK Activation Depends on PCK2

Pyruvate kinase metabolizes PEP generated from the PEP cycle as well as glycolysis. Oral glucose tolerance tests (OGTTs) assessed the extent to which PCK2 contributes to the action of PK activation *in vivo.* As with the hyperglycemic clamps, overnight fasted *Pck2*$^{-/-}$ mice had worse glucose tolerance compared to controls (Figure 1E). Initial insulin secretion was also worse in knockouts and dropped more rapidly in controls commensurate with plasma glucose (Figure 1F). We found that glucose tolerance following acute pretreatment with the PK activator TEPP46 (50 mg/kg; herein referred to as PKa) was improved for controls and could be explained by higher insulin release. In contrast, glucose tolerance with PKa treatment actually worsened in *Pck2*$^{-/-}$ mice, who also had worse insulin secretion compared to controls. Thus, both normal and PKa-amplified GSIS depend on PCK2.

We next assessed the beta cell intrinsic function of PCK2 directly by use of isolated islet perifusion experiments. We found that islet insulin content was not significantly different from *Pck2*$^{-/-}$ islets compared to controls (Figure S1I), but knockout islets had reduced first- and second-phase GSIS compared to WT littermate controls (Figures 2A and 2B). In the accompanying manuscript, acute application of PKa (10 μM) to INS1 832/13 cells, as well as mouse and human islets, amplified insulin release (Lewandowski et al., 2020). We also

found that PKa only stimulated insulin secretion from the control islets, confirming the dependence on PCK2-generated PEP for the PKa-mediated effect (Figures 2A and 2B).

Anaplerotic and PKa-Dependent Insulin Secretion Require PCK2

The cell-permeable methyl ester of succinate (SAME) oxidatively supplies electrons to complex 2 and at the same time supports anaplerosis and insulin secretion (MacDonald and Fahien, 1988; Malaisse-Lagae et al., 1994; Zawalich et al., 1993). In mouse islets, both SAME and PKa stimulated insulin release at 10 mM glucose (Figure 2C) with the combination being similar to that seen in human islets (Lewandowski et al., 2020). In contrast, PKa ± SAME did not stimulate secretion from *Pck2*$^{-/-}$ islets, indicating a dependence upon PCK2 function. Remarkably, despite poor GSIS, clamping *Pck2*$^{-/-}$ islets at 8 mM glucose (akin to second-phase secretion) resulted in a similar cytosolic calcium duty cycle (a measure of fractional time in the active oxidative phase of an oscillation) and oscillation frequency as that observed in control islets, though the amplitude was slightly lower in the KO islets (Figure 2D). The calcium response following acute glucose corresponds to first-phase secretion, and we found that it was also diminished in *Pck2*$^{-/-}$ (Figure 2E). At low glucose, the calcium response in mouse islets was especially sensitive to anaplerotic amino acids, a response that is muted as glucose dominates at higher concentrations (Lewandowski et al., 2020). Controls had a strong amino acid-stimulated calcium response that was further enhanced by PKa treatment (Figure 2F). *Pck2*$^{-/-}$ islets did not respond either to amino acids or to PKa treatment, demonstrating that both PK activation and anaplerosis require PCK2 to augment insulin secretion.

PKa Improves Insulin Secretion in Rodent and Human Models of Type 2 Diabetes

PKa amplified insulin secretion from insulinoma cells as well as healthy mouse, rat, and human islets in a glucose-dependent manner (Lewandowski et al., 2020). Multiple chemically distinct PK activators also amplified insulin release from human islets (Figure S2A), supporting an on-target mechanism. Male Sprague Dawley rats were fed a 4-week high-fat diet (HFD) prior to islet isolation and, like in healthy islets, acute treatment with AG-17540 (a structurally distinct [from PKa], cell-permeable, and orally bioavailable PK activator without taste aversion [unlike PKa] and herein referred to as PKa2) amplified GSIS from islets from HFD rats (Figure 3A) and KCl-depolarized islets (Figure S2B), consistent with both K_{ATP}-dependent and -independent mechanisms.

Although an HFD increases insulin resistance and causes dysglycemia, it does not precipitate diabetes in normal rats. However, the leptin-deficient Zucker rat develops HFD-induced diabetes (ZDF) compared to lean controls (ZF) (Figure S2C). Compared to ZF rats, islets from ZDF rats had lower islet insulin content and diminished second-phase insulin secretion during the glucose perifusion (Figures S2C, 3B, and 3C). Acute treatment of islets from ZDF rats with PKa improved both first- and second-phase insulin secretion (Figures 3B and 3C). In human islets, PKa amplified GSIS from four bona fide type 2 diabetes donors (Figure 3D).

Normal human islets were incubated for 72 h under glucolipotoxic (GLT) conditions (20 mM glucose + 1 mM 2:1 oleate:palmitate) to compare drug- and disease-related changes to

glucose-sensing (EC_{50} and maximal secretion) within a single donor (Figure 3E). PKa treatment of controls slightly lowered the EC_{50}, but maximal secretion was about 50% higher in contrast to GKa1 (PF-04967319, green curve), which lowered the glucose EC_{50} by ~3 mM into the hypoglycemic range but had only a slightly higher maximal secretion. In response to GLT (dashed lines), previously healthy islets maintained almost normal glucose sensing (EC_{50} 8.0 mM Con versus 7.0 mM GLT) but maximal insulin secretion was 70% lower. GKa further shifted the glucose sensing curve to the left (EC_{50} 3.5 mM) but did not restore maximal secretion. In sharp contrast, PKa recovered two-thirds of maximal secretion with minimal impact on EC_{50}.

Activating the PEP Cycle Improves Markers of Islet Function and Differentiation

After 3-day GLT exposure, the islet glucose-sensing mechanism remained intact and fully activatable by GKa (Figure 3E), while maximal secretion was impaired, suggesting a deficiency in insulin content and/or granule fusion. INS-1 cells and human islets exposed to either GLT or GKa1 for 3 days depleted islet insulin message and protein but had higher GK enzyme expression (Figures S2D–S2G). We found that insulin content was reduced in INS-1 cells and human islets from 7 donors treated with 2 GK activators (GKa1 or GKa2, MK-0941) for 3 days compared to control and PKa treatment (Figures 3F and 3G). We also found that markers of metabolic stress (e.g., *Txnip*) were higher in INS cells exposed to GLT, while markers of differentiation (e.g., *Mafa* and *Pdx-1*) were lower and worsened by GKa addition (Figure S2H). Three-day exposure of human islets to PKa did not impact overall GK protein levels (Figure S2G). PK enzymatic activity was not deficient (and was pharmacologically activatable) in islets from *Pck2*$^{-/-}$ mice and ZDF rats, and in GLT-treated human islets, indicating that reduced insulin secretion was not due to a primary PK deficiency per se (Figures S2I–S2K). To determine if PKa activation of the PEP cycle was also beneficial, we treated INS cells (Figures 3F and 3H) and human islets (Figure 3G) for 3 days with PKa ± GKa1 and GKa2, the SU tolbutamide (TBT), and the GLP1-RA exenatide (EX-4). While GK activator and TBT treatment depleted insulin message and protein content, to the contrary PKa raised them and mitigated the impact of GKa in INS-1 cells while insulin message was higher with EX-4 but to a lesser extent (Figures 3F–3H). In contrast to GKa, PKa did not reduce insulin content in human islets (Figure 3G). We found that the transcriptional profiling clearly segregated GKa1 and GKa2 from PKa and Ex-4 along the PC1 axis of the principle component analysis (Figure 3I). PKa, and to a lesser extent Ex-4, favored markers of beta cell health (e.g., higher *Ins1* and *2* and *Foxo1*, and lower *Txnip*) and maturity (higher *Mafa* and *Pdx1*) (Figures 3H and 3I) compared to GKa.

The glucose-induced gene *Txnip* increases with ER stress, glucotoxicity, and diabetes and may be an agent of beta cell failure (Shalev, 2014). *Txnip* was higher as expected from higher glucose metabolism with GKa treatment (Figures 3H, 3I, and S2H). Notably, this response was strongly suppressed by PKa alone or co-treatment relative to controls and GKa treatment despite the same ambient glucose concentrations (Figure 3H). These observations identify an unexpected role of PK activation in the protection of islets, both in terms of higher insulin protein and markers of differentiation and lower markers of beta cell stress and injury.

PKa Protects from *In Vivo* Islet Injury

Given the transcriptional changes observed with PKa treatment, to determine whether they were also associated with improved function independent of the acute metabolic activation, we treated INS cells for 72 h with drug and subsequent washout *prior* to assessing GSIS (Figure 3J). Prior PKa treatment had little to no residual impact on GSIS. In contrast to the GKa-induced dysfunction, we found that PKa mitigated the detrimental GKa injury. To determine if PKa was protective *in vivo*, rats were fed an HFD for 4 weeks ± twice daily oral PKa2 (25 mg/kg). After an overnight fast and without further drug exposure for 16 h (either *in vivo* or during the isolation), islets were isolated. Remarkably, *in vivo* PKa2-treated islets demonstrated amplified GSIS across the glucose concentration range tested (Figure 3K), without a reduction in islet insulin content (Figure S2L). As a control for retained drug following the isolation, human islets were cultured for 2 or 3 days with PKa and had identical GSIS performance following media exchange (Figures S2M and S2N). Taken together, targeting the PEP cycle with PK activation not only enhances insulin secretion but does so while improving markers associated with islet function and differentiation.

PK Activation Improves Insulin Secretion and Islet Health Markers *In Vivo*

Following an overnight fast, healthy male rats received a primed, continuous infusion of vehicle or either PKa or PKa2 with a target plasma concentration of ~10 μM (Figure S3A). As expected, under basal conditions neither fasting glucose nor insulin was altered in response to the drug infusion (Figures 4A and 4B). Following 90-min drug exposure, glucose concentrations were gradually ramped to a peak of 250 mg/dL over 70 min by a variable glucose infusion (Figure 4A). We found that both PK activators significantly improved insulin secretion once glucose was raised above 150 mg/dL (Figure 4B). A linear regression analysis demonstrated that both activators doubled GSIS at all points above this threshold (Figure S3B). Consistent with higher insulin secretion, the GIR was also higher in PK activator-treated rats (Figure S3C), accounting for higher glucose clearance (6–7 mg/kg·min).

HFD-fed rats were treated for 4 weeks with twice daily oral vehicle or PKa2 and then subjected to an overnight fast in the absence of further drug administration. A hyperglycemic ramp was performed but *without the further addition of drug.* We found that fasting and ramped plasma glucose concentrations were identical between both groups, but no difference in GIR was noted (Figures 4C and S3D). *In the absence of drug*, across basal and ramp conditions, plasma insulin levels were nearly doubled, reflecting preserved islet function (Figure 4D) that was independent of body weight and plasma glucagon (Figures S3E and S3F). Thus, PCK2-dependent activation of the PEP cycle via two chemically distinct, orally available small molecule PK activators improved islet function and maintained markers of health in preclinical diabetes models, in diabetic human islets, and up to 4 weeks *in vivo.*

PK Activation Short-Circuits Gluconeogenesis in Hepatocytes

Hepatic PKL, like PKM2, is activatable by PKa (Figures S4A and S5A) and would be predicted to increase PEP cycling to decrease gluconeogenesis. Primary hepatocytes from overnight fasted, chow-fed rats demonstrated a dose-dependent lowering (~60% at 10 μM)

of gluconeogenesis from 1 mM pyruvate and 9 mM lactate as substrates (Figure 5A). The reduction in gluconeogenesis was accompanied by a small (3%–5%), but statistically significant, increase in cellular respiration, consistent with a fractionally small futile cycle (Figure 5B). PEP concentration was significantly lowered in the hepatocytes treated with PKa; likewise, the PEP to pyruvate ratio was lower in PKa-treated hepatocytes (Figures 5C, 5D, and S4B). The pyruvate to lactate ratio and the sn-glycerol-3-phosphate (G3P) to dihydroxyacetone phosphate (DHAP) ratios were not different (Figures S4C and S4D), indicating that a shift in cytosolic redox did not explain the reduction in gluconeogenesis as proposed for metformin (Madiraju et al., 2014, 2018). Thus, PK activation reduces glucose production by short-circuiting gluconeogenesis in an energy-wasting metabolic futile cycle that provides an islet-independent mechanism for PKa to improve glucose homeostasis.

PK Activation Reduces Endogenous Glucose Production (EGP) *In Vivo*

Intravenous infusion of PKa in chow-fed overnight fasted rats did not change plasma glucose, insulin, glucagon, alanine, or glutamine (Figures 5E and S5B–S5E). Plasma lactate increased by 0.2 mM (Figure 5F), but was unassociated with an acidosis in blood gasses (pH, bicarbonate, or pCO_2; Figure S5F). During a primed-continuous intravenous infusion of [U-$^{13}C_6$]-D-glucose at each time, the study plasma M+6 glucose enrichments groups were identical until 30 min after concomitant PKa infusion (i.e., at t = ~120 min), when drug treatment increased the glucose enrichment (Figure 5G). Just as in the hepatocytes (Figure 5A), we found that the glucose rate of appearance (R_a) was acutely lowered (Figure 5H), indicating PKa reduced EGP. The normalized appearance of glucose label into lactate, alanine, and glutamine was not different (Figure 5I). Since plasma [glutamine] and [alanine] did not change, this indicates that the hydrolysis arm of the glucose-alanine and glucose-glutamine cycles were not changed by PKa treatment. For lactate enrichments to stay the same, even though plasma [lactate] increased by ~25% (Figure 5J), Cori cycle lactate production rate increased to a similar extent.

The muscle M1 isoform of PK does not respond to activation by PKa, making muscle a less likely explanation of increased lactate production. In contrast, RBCs respond to PKa as, like PKL and PKM2, the RBC isoform (PKR) is activated by PKa. RBCs lack mitochondria, which limits lactate generation to fermentative glycolysis augmented by the Luebering-Rapoport shunt (Figure S5G). We found that aside from PEP, PKa did not change RBC glycolytic metabolite concentrations (Figure S5H). In contrast, precursor-normalized RBC M+3 lactate enrichment quickly increased following PKa administration (Figure 5K). By isotope balance, plasma and RBC lactate are in reversible exchange with each other via the monocarboxylate transporter (MCT). To assess whether increased RBC lactate enrichment came from RBC glycolysis rather than uptake from the plasma, we compared the time course of the ratio of RBC M+3 lactate to plasma M+6 glucose, as well as the ratio of plasma to RBC M+3 lactate enrichments (Figures 5J–5L). In both measures, PKa accelerated RBC glycolytic lactate production relative to peripheral conversion.

The mechanism through which PK activation reduces EGP is encoded in the reappearance of the [U $^{13}C_6$]-glucose-derived M+3 lactate label back into glucose isotopomers via gluconeogenesis. The isotopologues of the mitochondrial-derived those precursors from

gluconeogenic tissues can be deconvolved via a mass isotopomer distribution analysis (MIDA; Equations 1, 2, 3, and 4) of the glucose isotopologues. Despite the higher precursor plasma M+6 glucose enrichment following PKa treatment, the M+3 those enrichment in liver was actually reduced, indicating reduced gluconeogenic flux (Figure 6A). As M+3 lactate enters the mitochondria, gluconeogenic PEP isotopomers are generated as a function of the relative contributions of TCA cycling, PEP cycling, and PC (Figure 6B). PEP cycling relative to the TCA cycle amplifies the M+2/M+3 ratio since the [(2,3) $^{13}C_2$] PEP isotopomer progressively accumulates with PK action. Consistent with its proposed mechanism of action, PKa treatment increased the M+2/M+3 triose ratio (Figure 6C).

In order to measure the relative contributions of the different *in vivo* cycling and gluconeogenic fluxes, we derived a model that incorporates the label from lactate recycling into glucose isotopomers (Equations 16, 17, 18, and 19). PKa treatment lowered the net lactate dehydrogenase (LDH) flux (V_{LDH}) into pyruvate relative to the citrate synthase rate (V_{CS}) and at the same time increased V_{PK} (Figure 6D). When assessed relative to PEPCK flux, rates of PEP cycling ($V_{PEPCycle}/V_{PCK}$) were nearly doubled while the mitochondrial gluconeogenic flux (V_{GNG}/V_{PCK}) was reduced by a third (Figures 6D and 6E). In response to activator treatment *in vivo*, PKa more than doubled the rate of PEP cycling relative to gluconeogenesis ($V_{PEPCycle}/V_{GNG}$) (Figure 6E).

The label dilutions of the mitochondrial-derived gluconeogenic precursors by unlabeled glycerol and glycogen were small and not different between the two groups when comparing measured versus MIDA-predicted higher-order glucose isotopomers. As such, the absolute *in vivo* rates of the cycling and gluconeogenic fluxes were determined (Figures 6F and 6G; Equations 20, 21, 22, 23, and 24) by bootstrapping onto the glucose R_a (Perry et al., 2015). Thus, in absolute terms, the observed reduction in EGP *in vivo* is mechanistically explained by decreased mitochondrial gluconeogenesis (V_{GNG}) as PC flux (V_{PC}) gets diverted into PEP cycling ($V_{PEPCycle}$) via acute PK activation. Given the short duration of drug exposure, these data are consistent with on-target activation of PK metabolism of PEP into pyruvate that short-circuits gluconeogenesis.

Liver PK Activity Is Reduced in Insulin Resistance

We found that PK activity and protein expression were significantly lower in livers from two rodent models of insulin resistance, the 4-week HFD-fed rat (Figures 7A and 7B), and insulin receptor antisense oligonucleotide (ASO)-treated rats compared to controls (Figures S6A and S6B). Chronic HFD feeding also remodeled the PK phosphoforms away from a protein kinase A signature (less S12P) and toward the insulin-resistant cyclin-dependent kinase (CDK) signature (increased S113P) (Figures 7C and 7D). Concomitant PKa2 treatment lowered S113P but did not change S12P (Figures 7E and 7F). So in contrast to islets, a reduction in hepatic PK activity and S113P is associated with insulin resistance and is modifiable with PK activation.

Chronic PKa during an HFD Improves Insulin Sensitivity and Reduces Ectopic Fat

To examine if the chronic activation of PK impacts whole-body energy metabolism, we performed metabolic cage studies for HFD-fed mice treated with the non-taste-averse PK

activator, PKa2. Consistent with the lack of change in body weight, 4-week treatment with PKa2 did not alter oxygen consumption, carbon dioxide production, respiratory quotient, energy expenditure, feeding, and activity during metabolic cage studies (Figures S6C–S6I). To assess intra- and inter-tissue glucose homeostasis, rats were placed on a similar 4-week HFD and treated twice daily with oral PKa2 or vehicle. We then examined the rats after an overnight drug washout and fast to determine if *prior* drug treatment protected against the development of insulin resistance. There was no difference in fasting plasma glucose, insulin, non-esterified fatty acids (NEFAs), fatty acid turnover, liver enzymes, or body weight (Figures S6J–S6O and S3E) in either cohort. Importantly, basal EGP (R_a) was 15% lower in the cohort with prior-PKa treatment (Figure 7G). Plasma and liver triglyceride (TAG) were significantly reduced by prior PK activator treatment during the HFD (Figures 7H and 7I), while insulin-stimulated protein kinase B (AKT) phosphorylation was significantly higher (Figure 7J). It is possible to decrease hepatic lipids by reducing lipolytic rates in adipose (Girousse et al., 2013). However, basal and clamp plasma NEFA concentrations and fatty acid turnover were not altered (Figures S6L and S6M). Together with reduced basal Ra and the modified PK phosphoforms, these data strongly indicate that activation of PKL improves liver insulin resistance.

Notably, the GIR was higher in the prior-PKa-treated group during hyperinsulinemic-euglycemic clamps (Figure 7K), leading to a 20% increase in peripheral glucose disposal rates (Figure 7L). As noted, the muscle PKM1 isoform does not respond directly to PK activation, and in the absence of drug, RBCglycolysis would not be accelerated to explain the increased glucose disposal rate. However, muscle TAG content was decreased while muscle glycogen and AKT and insulin receptor phosphorylation were increased (Figures 7M–7P). These whole-body studies demonstrate that oral pharmacologic activation of the L, R, and M2 isoforms has the unique properties of improving islet function without injury and improving insulin sensitivity. These are favorable qualities for a potential pharmaceutical target in diabetes and potentially other metabolic diseases.

DISCUSSION

A number of successful therapeutic strategies for the treatment of type 2 diabetes have included augmenting islet output, as well as reducing insulin resistance. Here, we show that PK activation directly improves both. PK activation improves islet function, and importantly, this improvement is within the physiologic glucose range. PK activation also works synergistically in other tissues to improve hepatic and peripheral insulin resistance. [U-$^{13}C_6$]-D-glucose-based metabolic measurements demonstrated acute PKa treatment improved *in vivo* metabolism by increasing the (1) glucose R_a; (2) flow through the Cori (glucose-lactate), glucose-alanine, and glucose-glutamine cycles; (3) reappearance into glucose through gluconeogenic and PEP cycling fluxes; and (4) transit through RBC glycolysis. Indeed, this is the first therapeutic strategy we are aware of where some of the improvement in glucose homeostasis may be attributed to accelerated RBC metabolism.

The last step of glycolysis generates pyruvate, which, due to the restricted expression of LDH in beta cells, has only two potential dispositions: entry into oxidative metabolism via PDH or entry into anaplerotic pathways via PC (Schuit et al., 2012). Therefore, with a

constant influx of glucose carbon, accelerating PDH is expected to increase glucose oxidation at the expense of anaplerotic pathways (Jensen et al., 2008; MacDonald and Chang, 1985a; MacDonald et al., 2005; Prentki et al., 2013). The DCA and PDKdKO data confirm that diverting the balance of pyruvate away from anaplerosis and into oxidative metabolism through inhibition of PDK would not be an effective therapeutic strategy to improve islet function.

The current consensus model for beta cell glucose sensing, where GK exerts control over OxPhos, does not predict a beneficial impact from PK activation on insulin secretion (Matschinsky and Ellerman, 1968). Instead, PK-dependent glucose sensing is mechanistically dependent on anaplerotic metabolism (e.g., PC, amino acids, or SAME) coupled to PK through PEP produced by the mitochondrial GTP-dependent enzyme PCK2. Increased mtGTP synthesis accelerates the PEP cycle to increase insulin secretion that, counterintuitively, was also accompanied by higher insulin content, increased differentiation, and resistance to metabolic toxicity (Jesinkey et al., 2019).

Compared to oxidative flux through PDH, anaplerosis through PC more steeply correlates with insulin secretion (Alves et al., 2015; Cline et al., 2004; Lu et al., 2002; MacDonald and Chang, 1985b; Newgard et al., 2002; Pongratz et al., 2007; Prentki et al., 2013). Pyruvate oxidation, the cornerstone of the consensus model, does not change the concentration of TCA intermediates because each OAA consumed to make citrate is regenerated, completing the cycle. In contrast, anaplerosis expands the TCA metabolite pool size through net synthesis of OAA while cataplerosis counterbalances this metabolite excess by exporting metabolites to shrink the TCA pool size. Pyruvate anaplerosis is mechanistically linked to cataplerosis of OAA by the synthesis of PEP in the PEP cycle (Jesinkey et al., 2019; Stark et al., 2009). Since beta cells do not have cytosolic PEPCK (PCK1), non-glycolytic synthesis of PEP depends on the reaction of mtGTP with anaplerotic OAA via PCK2 (Figure 1A) (Jesinkey et al., 2019; MacDonald and Chang, 1985a; MacDonald et al., 1992; Stark et al., 2009). The importance of mtGTP synthesis was demonstrated *in vivo* and *in vitro* (Jesinkey et al., 2019; Kibbey et al., 2007), but prior to the *Pck2*$^{-/-}$ studies, the involvement of PCK2 cataplerosis in beta cell function had only been supported in insulinoma cells *in vitro* (Jesinkey et al., 2019; Stark et al., 2009).

Islet failure is likely not attributable to a single step in the glucose-sensing mechanism. Nevertheless, the distinction between oxidation and anaplerosis/cataplerosis is important as increased islet glucose metabolism can be a double-edged sword: initially augmenting function, but eventually harming beta cells over time. While GK governs glucose entry into beta cell metabolism, it is not subject to product inhibition like other hexokinases (Matschinsky and Ellerman, 1968) as glucose is pushed into metabolism. Pharmacologic GK activators lower the EC_{50} for glucose and have advanced with limited success in human trials as a potential diabetes treatment because of hypoglycemia and hypermetabolic islet injury (De Ceuninck et al., 2013; Efanova et al., 1998; Erion et al., 2014; Iwakura et al., 2000). A general concern, then, is that strategies enhancing glucose metabolism could potentially have long-term negative consequences. Accordingly, there has been diminished enthusiasm for therapies directed at only improving islet function for concerns of islet

overwork injury from insulin secretagogues or alternatively concern that hyperinsulinemia per se worsens insulin resistance (Titchenell et al., 2017).

As an alternative, pharmacologically redirecting metabolic traffic downstream of GK may actually reduce oxidative damage while at the same time improving function. Consistent with this, PKa in INS cells and human islets did not significantly impact oxygen consumption (Lewandowski et al., 2020). In both normal and GLT conditions, PK activation in insulinomas and mouse, rat, and human islets mechanistically distinguished itself from GK activation by improving maximal insulin secretion without lowering the stimulation threshold into the hypoglycemic range. This glucose dependency minimizes the risk of hypoglycemia similar to GLP1R agonists, but distinct from the increased risk from GK activation or SU receptor agonism. Redeeming features of pharmacologic PK activation *in vivo* include that insulin secretion into the portal vein is only amplified when glucose is high (>150 mg/dL in rats), there is no basal hyperinsulinism, and beta cell health is still protected. As such, PK activation in the setting of an HFD challenge preserved appropriate islet function and important markers of islet health such as insulin content and, thus, should be distinguished therapeutically from the potentially pathologic hyperinsulinemia from secretagogue or subcutaneously administered insulin.

The data here do not exclude other potential islet signaling metabolic pathways that either intersect with the PEP cycle or work through other mechanisms to increase insulin secretion. K_{ATP}-independent mechanisms may rely on metabolic features related to the size of the readily releasable pool of insulin granules or their priming (Ferdaoussi et al., 2015; Olofsson et al., 2002). Anaplerotic PC metabolism was identified as part of the beta cell glucose sensing mechanism nearly three decades ago (reviewed in Jensen et al., 2008; MacDonald et al., 2005). The only other PC-dependent anaplerotic pathway, besides the PEP cycle, involves the synthesis of pyruvate from malate via malic enzyme to generate cytosolic NADPH (Pongratz et al., 2007). While the malic enzyme pathway is diminished in genetic models that increase mtGTP to amplify insulin secretion (Jesinkey et al., 2019), this does not rule out other potential PC-dependent pathways. In beta cells, neither *de novo* lipogenesis nor G3P synthesis depends on anaplerosis. Nevertheless, evidence also supports a G3P-consuming fatty acid cycle that stimulates insulin secretion via the generation of lipid second messengers (Prentki et al., 2013).

This work did not identify an underlying islet PK deficiency per se contributing to beta cell dysfunction and may even argue against it. Furthermore, given that endogenous regulation of PK includes substrate availability, allosteric activation, and post-translational modification (Harris and Fenton, 2019), other secondary deficiencies in PK have not yet been excluded as a contributor to islet glucolipotoxicity. In contrast to islets, there were relative HFD-induced PK deficiencies and altered PK phosphoforms in the liver that were modifiable by pharmacologic PK activation. Notably, human PKL polymorphisms are associated with T2D, PK activity is downregulated in diabetes, and insulin itself regulates PK activity (Miyanaga et al., 1982; Parks and Drake, 1982; Wang et al., 2002). PK deficiency is also associated with severe liver dysfunction in newborns (Staal et al., 1982).

During gluconeogenesis, two nucleotide triphosphate-consuming steps generate PEP from pyruvate. In the liver, PK guards the highly energetically favorable PEP hydrolysis with the potential to completely short-circuit gluconeogenesis. Both glucagon (via protein kinase A) and HFD feeding (via CDK signaling pathways) increase glucose production in part by limiting an energetically favorable metabolic short-circuit in which PEP is hydrolyzed back to pyruvate by PKL. We recently reported that short periods of diet-induced insulin resistance (3-day HFD) acutely increased PK expression and localization to the nucleus via CDK-mediated phosphorylation on the novel site S113P (Gassaway et al., 2019). Given that activation of PK improves both the production and clearance of glucose in control conditions, we now show that PK activity is diminished and associated with altered phosphorylation with longer durations of insulin resistance.

It is unclear at this time whether PK activation in the liver can induce mitochondrial ADP privation like it does in the beta cell (Lewandowski et al., 2020). The fact that V_{PC} did not increase following PK activation suggests that fasting hepatic mitochondria are already in the state-4-like "$Mito_{Synth}$" respiration that was observed to oscillate in beta cells.

PKa reduced gluconeogenic output by one-third not by slowing PC, but by redirecting PCK2 flux back toward pyruvate. Increased PEP cycling to pyruvate was accompanied by reduced V_{LDH} that could not be explained by a shift in the hepatic cytosolic redox potential but rather by mass balance. The energy wastage of the futile PEP cycle is mildly inefficient compared to chemical uncouplers or UCP1 induction. Consistently, a statistically significant (but minimally physiologically relevant) 3%–5% increase in OCR followed PK activation in hepatocytes, but nonetheless it was surprising to also see liver protection from TAG accumulation. Increased tissue TAG is a marker of hepatic insulin resistance in human subjects and rodent models of type 2 diabetes (Petersen et al., 2004; Samuel et al., 2010). Recently, PK-L in mouse liver was demonstrated to protect from the actions of high-fructose diet feeding on the liver, further supporting regulation of this metabolic step as a potential therapeutic target (Shi et al., 2020). As fat is the primary energy source oxidized in the liver, accelerating the energy-wasting futile PEP cycle could have the additional benefit of melting away pathologic ectopic intra-organ fat as seen in the diabetes-induced obesity model.

In addition to directly improving hepatic insulin resistance, the 4-week treatment with PKa2 had spillover benefits to tissues (i.e., muscle) lacking an activatable PK isoform. The muscle improvements correlated with diminished TAGs, suggesting PK activation had indirectly protected muscle from HFD-induced insulin resistance. These data are consistent with the correlation between reducing muscle TAG and improving skeletal muscle insulin responsiveness at the level of IRK (Yu et al., 2002). In general, mechanisms of insulin resistance are complex and contested, and thus additional work will be required to confirm the mechanism of these secondary benefits. Regardless, the protection afforded by prior PK activation during HFD feeding was accompanied by diminished ectopic fat, increased muscle glycogen, improved insulin signaling, reduced basal glucose production, and enhanced insulin-stimulated glucose disposal. Outside of diabetes, these may have potential value to diseases accompanied by ectopic lipid accumulation, such as NAFLD and NASH.

As shown in the companion manuscript (Lewandowski et al., 2020), the PK-catalyzed reaction harnesses the free energy of PEP hydrolysis to cause ADP privation of both the mitochondria and KATP channels that depolarizes the plasma membrane. The PK activator AG348 has been demonstrated to be well tolerated in Phase 1 healthy volunteer studies and a Phase 2 trial in patients with PK deficiency (Grace et al., 2019; Yang et al., 2019). This therapy was advanced to treat symptomatic RBC glycolytic deficiency leading to hemolytic anemia in patients with genetically derived PK-R deficiency. In our study, healthy rodents with normal levels of PK-R still demonstrated accelerated RBC fermentative glycolysis with acute PK activation that explains at least part of the observed metabolic benefit. In bypassing ATP synthesis by phosphoglycerate kinase, the Luebering-Rapoport shunt in RBCs is also an energy-wasting pathway with a lower yield of ATP per glucose (Figure S5H). It is worth noting that differences in RBC metabolites have recently been demonstrated, with 2,3 bisphosphoglycerate increased in diabetes compared to healthy subjects (Palomino-Schätzlein et al., 2020). The extent to which RBCs, as a circulating, metabolically active ~2.5 L tissue, can be safely harnessed in humans to improve whole-body glucose homeostasis remains an intriguing possibility.

At the therapeutic dose, the two PK activators used in this study did not discriminate between PKM2, PKL, or PKR, and it is unclear whether there could be additional advantages to favoring particular isoforms of PK and/or targeting specific tissues where they are expressed. Perhaps it is not surprising that the PEP cycle, given that it integrates glycolytic, gluconeogenic, oxidative, anaplerotic, and cataplerotic metabolism, is an important whole-body regulatory control point governing central carbon metabolism in multiple tissues. Here we provide supporting preclinical data that the concerted PK activation in beta cells, liver, RBCs, and potentially other tissues may be beneficial in diseases, such as type 2 diabetes, where glucose metabolism is aberrant.

Limitations of Study

This manuscript focuses on the PEP cycle as a single, but important, component of a complex, tunable, and interconnected mechanism by which beta cells are able to sense glucose, other nutrient signals, and other regulatory responses. As such, these studies are not designed to exclude other contributing nutrient-sensing mechanisms. Likewise, mechanisms of insulin sensitivity are equally if not more complex and contentious and may vary between tissues and species or condition. Future directed studies will be required to characterize the mechanisms underlying some of the observations, such as the alterations in tissue and plasma lipids. Further, because structurally different PK activators elicited similar responses in this study and Lewandowski et al. (2020), that their pharmacology has largely been interpreted as “on target” at the doses used does not rule out non-metabolic “on-target” responses, secondary responses, or off-target responses, nor does it distinguish the individual PK isoform (aside from excluding PKM1) or tissue-specific contributions *in vivo.* While markers of improved islet function and differentiation were suggestive of improved islet health, longer-term dietary or genetic model studies (e.g., *db/db* mice or ZDF rats) with head-to-head comparisons with established comparators (e.g., GLP-1R agonists) with and without washout will be required to document whether the observed markers of islet health actually translate into clinically relevant preservation of islets. Physiologic and

pharmacologic observations made in cell lines, rodents, and isolated human islets may vary between species and conditions, and thus PK activation as an anti-diabetic approach will eventually have to be confirmed in human studies.

STAR★METHODS

RESOURCE AVAILABILITY

Lead Contact—Further information and requests for resources and reagents should be directed to and will be fulfilled by the Lead Contact, Richard Kibbey Richard.Kibbey@yale.edu

Materials Availability—Mouse lines generated in this study (*Pck2*$^{+/+}$ and *Pck2*$^{-/-}$ mice) are available from the lead contact upon request.

PKa2 can be obtained directly from Agios under MTA or is available to purchase from commercial online as compound 162842801-2.

Data and Code Availability—This study did not generate any unique datasets or code.

EXPERIMENTAL MODEL AND SUBJECT DETAILS

All animal studies were approved by the Yale University Institutional Animal Care and Use Committee and were performed in accordance with all regulatory standards. Healthy 240-260 g male Sprague-Dawley rats were obtained from Charles River Laboratories (Wilmington, MA) were first acclimated to the in the Yale Animal Resources Center at 23°C under 12 h light/12 h dark cycles (0700–1900 h) and single housed while they were fed either a high-fat diet (Research Diet D12492, New Brunswick, NJ; 60% calories from fat, 20% from carbohydrate, 20% from protein) ad lib for 4 weeks or a regular chow diet (Harlan Teklad #2018, Madison, WI; 18% calories from fat, 58% from carbohydrate, 24% from protein). HFD-fed rats were treated twice daily (observed) for 4 weeks with PK activator (25 mg/kg) in peanut butter or peanut butter vehicle while they were maintained on the HFD diet. Detailed information of PKa activators, PKa (TEPP46) and PKa2 (AGI-17540), are provided in the Key Resources Table. Rats underwent the placement of jugular venous catheters for blood sampling and carotid artery for infusion ~7 days before the terminal studies and recovered their pre-surgical weights by 5-7 days after the operation. All infusions were performed on overnight fasted rats. At the end of each study, rats were euthanized by IV pentobarbital.

All strains were on a C57BL/6J background and male mice were studied at 8 to 9 weeks of age. Healthy male mice for the metabolic cage studies were purchased from Jackson Laboratory and acclimated prior to study. All of the *Pck2*$^{-/-}$ and wild-type (WT) littermate mice were bred and maintained at Yale and fed on a regular chow diet (Harlan Teklad TD2018:18% fat, 58% carbohydrate, and 24% protein). Study cohorts consisted of homozygous *Pck2*$^{-/-}$ mice and littermate male WT controls. All mice received *ad libitum* access to food and water and were bred, maintained and housed in the Yale Animal Resources Center at 23°C under 12 h light/12 h dark cycles (0700–1900 h). Catheters were

placed in the jugular vein 6 - 9 days before the experiments; only mice that recovered more than 95% of their pre-operative body weight were studied.

***Pck2*$^{-/-}$ Mouse—**Heterozygous PCK2 knockout mice (denoted C57BL/6NTac-Pck2$^{tm1\ (KOMP)Vlcg}$, project ID VG13655) were obtained from the University of California Davis Knockout Mouse Project repository. For these knockout mice the VelociGene targeting strategy was employed, which enables the rapid and high-throughput generation of custom gene mutations in mice according to method described previously (Dechiara et al., 2009; Valenzuela et al., 2003). The insertion of Velocigene cassette ZEN-Ub1 created a deletion of size 8372bp between positions 55548778-55540407 of Chromosome 14. Mice harbor a gene expression reporter *(lacZ)*, and mice had a neomycin cassette. At the Monash Animal Research Facility heterozygous knockout mice were crossed with CMV-Cre mice, which express Cre recombinase under the CMV promoter, to delete the loxP flanked selection cassette, and to generate global neomycin cassette-free PCK2 knockout mice. Heterozygous PCK2 knockout mice were further crossed with C57BL/6J mice to create PCK2 knockout mice on a C57BL/6J background. Offspring that inherited the targeted PCK2 allele were interbred as heterozygotes for production of experimental *Pck2*$^{+/+}$ and *Pck2*$^{-/-}$ mice. *Pck2*$^{-/-}$ mice behave normally and are viable and fertile.

METHOD DETAILS

In Vivo Studies

Hyperglycemic Clamp Studies: In hyperglycemic clamp studies, overnight-fasted, awake mice under gentle tail restraint were infused with 20% D-glucose at a variable rate to maintain hyperglycemia (240–260 mg/dl). Plasma glucose was measured using an Analox GL5 Analyzer (Analox Instruments, UK). Serum insulin was measured via Mouse Ultrasensitive ELISA (80-INSMSU-E01, ALPCO). Fasting serum glucose and insulin concentration were also measured using the same methods, respectively.

For acute PKa treatment and hyperglycemic clamp.: One week prior to experimentation, chow-fed male SD rats (~300 g) underwent surgical arterial and venous catheterization. After recovering from surgery, rats were fasted overnight and received an intravenous bolus of compound PKa (11 mg/kg), PKa2 (11mg/kg) or vehicle control followed by a continuous infusion with compound PKa or PKa2 @ 0.17 mmol/kg/min throughout the entire infusion study. At 90 min, 20% dextrose was infused at a variable rate to reach hyperglycemia (240 - 260 mg/dl). Blood samples (50 μl) were taken every 15 min for measurement of glucose using a Ana Analox GL5 glucose analyzer.

For chronic PKa2 treatment and hyperglycemic clamp.: Observed individual treatment of HFD-fed rats with PKa2 was performed twice a daily for 4 weeks with 25 mg/kg in peanut butter or peanut butter vehicle. HFD-fed rats treated with PKa2 were overnight fasted to start the experiment and the PKa2 in peanut butter was given before the overnight fasting. Plasma samples were collected before the start of infusion (basal 0 min) to measure glucose and insulin levels. Rates of infused 20% glucose was variably increased as shown to reach target hyperglycemia while collecting plasma samples at 15, 30, 45, 60, 75, 90 min.

Chronic PKa2 treatment and Hyperinsulinemic clamp.: Following an overnight fast, a 120-min basal infusion of (U-$^{13}C_6$) glucose (1 mg·kg^{-1} · min^{-1} prime continuous infusion) was administered, with 200 μL of whole blood taken after 120 min of infusion to measure glucose turnover. Immediately following the basal infusion, 120-min hyperinsulinemic-euglycemic clamps were performed. Rats received arterial infusions of insulin (prime: 40 mU/kg over 5 min; followed by a continuous dose: 4 mU·kg^{-1} · min^{-1}) for the duration of the clamp. Euglycemia (100–110 mg/dl) was maintained with a variable infusion of uniformly labeled [U-$^{13}C_6$]-d-glucose. Blood samples (50 μl) were taken every 15 min for measurement of glucose using a An Analox GL5 glucose analyzer. After 120 min, rats were euthanized with intravenous pentobarbital, and tissues were rapidly freeze-clamped in aluminum tongs precooled in liquid N_2. [U-$^{13}C_6$]-D-glucose enrichment were measured by GC/MS as previously reported (Perry et al., 2015), and turnover was calculated using the formula: Turn over = [(^{13}C tracer enrichment /^{13}C plasma enrichment)-1]*infusion rate.

Acute PKa Actions on Glucose Turnover: The acute actions of PKa on EGP in overnight fasted regular chow-fed rats were tested with a primed, continuous infusion of PKa and assessed with [U $^{13}C_6$]-D-glucose tracer. At time 0, glucose label was introduced into the doubly catheterized rats via a continuous, unprimed infusion 1 mg/kg/min rate and sampled at the indicated times. Plasma was immediately separated from RBCs and both frozen for separate analysis by LC/MS/MS and GC/MS. At 90 min, a primed, continuous PKa versus vehicle infusion was initiated for the remainder of the study.

Oral Glucose Tolerance Test (OGTT): Glucose tolerance tests were performed after an overnight fast. Mice were intraperitoneally injected with PKa with 50 mg/kg. After one h of PKa injection, mice were gavaged with 1 g/kg glucose, and blood was collected by tail bleed at 0, 15, 30, 45, 60, and 120 min for plasma insulin and glucose measurements. Plasma glucose concentrations were measured using the glucose oxidase method on an Analox GL5 Analyzer (Analox Instruments, UK). Serum insulin was measured via Mouse Ultrasensitive ELISA (80-INSMSU-E01, ALPCO). Fasting serum glucose and insulin concentration were also measured using the same methods, respectively.

Metabolic Cage Studies: Mice on the C57BL6 background were randomly divided into 2 groups. Mice were maintained on the HFD diet while they were treated daily with PKa2 mixed in peanut butter, or peanut butter vehicle, at the dose specified (50 mg/kg) daily for 4 weeks. All mice consumed the peanut butter with or without PKa2 within 2 min. Lean body mass was assessed by 1H-magnetic resonance spectroscopy (Bruker BioSpin, Billerica, Massachusetts). Comprehensive Lab Animal Monitoring System (CLAMS; Columbus Instruments, Columbus, Ohio) was used to evaluate O2 consumption, CO2 production, energy expenditure, activity, food consumption and drinking.

Whole Body Lipolytic Rates: Following an overnight fast, a 120-min basal infusion of [U-$^{13}C_{16}$]-palmitate [0.2 mmol/[kg·min] prime continuous infusion, Cambridge Isotopes] was administered, with 200 μL of whole blood taken after 120 min of infusion to measure basal fatty acid turnover. Immediately following the basal infusion, 120-min hyperinsulinemic-euglycemic clamps were performed. Rats received arterial infusions of

insulin (prime: 40 mU/kg over 5 min; followed by a continuous dose: 4 mU·kg−1·min−1) for the duration of the clamp. GC/MS was used to measure [U-$^{13}C_{16}$] palmitate enrichment, from which we calculated the rates of lipolysis we have described (Perry et al., 2015; Vatner et al., 2015).

In Vivo *Plasma and Red Blood Cell Measurements*: Regular-chow-fed rats were overnight fasted before experiment and was infused [U $^{13}C_6$]-D-glucose tracer (1 mg/kg/min). At time 90 min, rat received an intravenous bolus of compound PKa (11 mg/kg) or vehicle control followed by a continuous infusion with compound PKa 0.17 μmol/kg/min throughout the entire infusion study. Plasma was immediately separated from red blood cells (RBCs) and both frozen for separate analysis by LC/MS/MS and/or GC/MS.

Cell and Tissue Studies

Hepatocyte Studies: Primary hepatocytes from regular chow rats were isolated at the Yale Liver Center. Cells were washed three times with recovery media (DMEM with high glucose plus 10% FBS), and an equal number of cells were seeded in each well of a 6-well plate. Isolated hepatocytes were suspended and washed two times in recovery medium containing DMEM high glucose (20 mM) (Sigma, D5648) with 10% FBS, 1 nM insulin, 1 nM dexamethasone, and antibiotics (10,000 units/mL penicillin and 10 mg/mL streptomycin, Invitrogen). Cell count and viability were estimated by trypan blue exclusion. The cells were plated at 5×10^5 cells/cm^2 in collagen-I-coated (BD Biosciences) 6-well plates in recovery medium and were cultured under 5% CO_2 and 95% O_2 in air at 37°C. After 4 h, cells were washed with PBS, and the medium was changed to DMEM low glucose (5 mm) (Sigma, D5921) with supplemented antibiotics but no hormones prior to gluconeogenesis assays. Hepatocytes were incubated in the presence and absence of substrate (Pyruvate 1mM, lactate 9 mM) and drug as indicated in DMEM (D5030, Sigma) with 2 mM L-glutamine and 24 mM bicarbonate without glucose. After 3 h the medium was removed for enzymatic analysis of glucose, background subtracted and normalized to the protein content. PK activity in the lysate was measured as described.

Oxygen Consumption Measurement: Isolated hepatocytes (12,000 per well) were seeded into a Seahorse XF96 cell culture plate (Agilent Technologies) after having been coated with collagen. Cells were kept in recovery media for 4 – 6 h and then washed with DMEM media (low glucose plus 10% FBS) and incubated overnight (DMEM low glucose (5 mM) with 10% FBS, 1 nM insulin, 1 nM dexamethasone, and antibiotics (10,000 units/mL penicillin and 10 mg/mL streptomycin, Invitrogen). The following morning, cells were washed and incubated in 180 μL of prewarmed (~37°C) DMEM base media (D5030, Sigma) supplemented with 2mM L-glutamine, 24mM bicarbonate, 10mM HEPES and 0.2% BSA with or without PKa 10μM and equilibrated in a ~37°C non CO2 incubator for 1 h prior to the study. Basal oxygen consumption was observed followed by the addition of the gluconeogenic substrate combination of pyruvate (1 mM) and lactate (9 mM). Chemical stimulants for assessing mitochondrial function were subsequently injected following the substrate addition in the following order; oligomycin 5 μM, FCCP 10 μM and rotenone 5 μM. Measurements of oxygen consumption rate were taken, and the average of the measurements after each injection was used for analysis.

Measurement of Total Glycogen: 100 mg skeletal muscle tissue was homogenized in lysis buffer. Samples were centrifuged at 5000 × *g* for 5 min at 4°C. 100 μL of the supernatants or glycogen standards (0–200 μg) were spotted onto GF/A filters. Filters were washed in ice-cold 70% ethanol for 15 min followed by two 10-min washes in 70% ethanol at room temperature. After drying overnight, filters were placed in 13 × 100-mm glass tubes and incubated with 1 mL of amyloglucosidase (0.04% in 0.05 M sodium acetate) for 90 min at 37°C. Glucose present in 100 μL of the reaction was analyzed by using a Glucose-SL assay (Sekisui Diagnosis, lot: 49811).

Plasma Assays and Tissue Lipid Measurement: Standard kits were used to measure plasma non-esterified fatty acids (Wako) and triglycerides (Sekisui). Tissue triglycerides were extracted using the method of Bligh and Dyer and measured using a standard kit (Sekisui).

Islet Studies

Islet Isolation and GSIS: Pancreata were excised from anesthetized rodents (rats and mice) and islets were isolated by collagenase P digestion followed by centrifugation with Histopaque 1100 solution for density separation of pure islets and then hand-picked as previously described (Kibbey et al., 2014). Islets were allowed to recover for 24 - 48 h in RPMI with 10% FBS and antibiotics with either 5 mM glucose (rats) or 11 mM glucose (mice). Approximately 50-80 islets were then layered between a slurry of acrylamide gel column beads (Bio-Gel P4G; BioRad150-412) and perifusion buffer DMEM (D-5030, Sigma) supplemented with 24 mM $NaHCO_3$, 2.5 mM glucose, 10 mM HEPES, 2 mM glutamine and 0.2% fatty acid-free BSA. The islets were perifused at 100 ml/min for a 1 h equilibration period using a Bio-Rep Perifusion Instrument (Miami, FL) that maintains precise temperature, gas (5% CO2/95% air) and flow control. After the stabilization period, the islets were perifused with 2.5 mM glucose for 10 min followed by stimulatory glucose 9 mM (rat) or 16.7 mM (mouse) for 45 min followed by 30 mM KCl as indicated. During the perifusion, outflow was collected into a 96-well plate format and secreted insulin concentrations were measured by a high range rodent insulin ELISA assay kit (ALPCO) and normalized to islet DNA which was measured using the Quant-iT PicoGreen dsDNA Reagent (Life Technologies Corporation).

Time Lapse Imaging: For measurements of cytosolic Ca^{2+}, islets were pre-incubated in 2.5 μM FuraRed (Molecular Probes F3020) in islet media for 45 min at 37°C before they were placed in a glass-bottomed imaging chamber (Warner Instruments) mounted on a Nikon Ti-Eclipse inverted microscope equipped with a 20X/0.75NA SuperFluor objective (Nikon Instruments). The chamber was perfused with a standard external solution containing 135 mM NaCl, 4.8 mM KCl, 2.5 mM $CaCl_2$, 1.2 mM $MgCl_2$, 20 mM HEPES (pH 7.35). The flow rate was 0.4 mL/min and temperature was maintained at 33°C using solution and chamber heaters (Warner Instruments). Excitation was provided by a SOLA SEII 365 (Lumencor) set to 10% output. Single DiR images utilized a Chroma Cy7 cube (710/75x, T760lpxr, 810/90 m). Excitation (430/20x and 500/20x) and emission (630/70 m) filters (ET type; Chroma Technology) were used in combination with an FF444/521/608-Di01 dichroic beam splitter (Semrock) and reported as the excitation ratio (R430/500). Fluorescence

emission was collected with a Hamamatsu ORCA-Flash4.0 V2 Digital CMOS camera every 6 s. A single region of interest was used to quantify the average response of each islet using Nikon Elements and custom MATLAB software (MathWorks).

Human Islet Insulin Secretion Studies: Human islets from normal and Type 2 diabetic donors obtained from the University of Alberta Diabetes Institute, the University of Chicago Diabetes Research and Training Center, or Prodo Laboratories (CA) were cultured in glutamine-free CMRL supplemented with 10 mM niacinamide and 16.7 μM zinc sulfate (Sigma), 1% ITS supplement (Corning), 5 mM sodium pyruvate, 1% Glutamax, 25 mM HEPES (American Bio), 10% HI FBS and antibiotics (10,000 units/mL penicillin and 10 mg/mL streptomycin). All media components were obtained from Invitrogen unless otherwise indicated. Human donor islets were cultured intact, then dispersed and reaggregated as pseudo-islets for dynamic insulin secretion studies. Islets were dispersed with Accutase (Invitrogen) and the resulting cell suspension was seeded at 5000 cells per well of a 96-well V-bottom plate, lightly centrifuged (200g) and then incubated for 12 - 24 h at 37°C5%, CO_2 95% air for the islet to reform into an intact islet. Dynamic GSIS studies were performed 24 h after the islets were plated into the 96 well plates following dispersion and re-aggregation. The human islet plates were washed and incubated at 37°C5% CO_2, 95% air in DMEM (D5030, Sigma) supplemented with 24 mM $NaHCO_3$, 2.5mM glucose, 10 mM HEPES, 2 mM glutamine and 0.2% fatty acid-free BSA for 1.5 h. After the first incubation, human islet plates were then washed with glucose free study DMEM and incubated for 2 h in DMEM study media with 1, 2.5, 5, 7, 9, 11.2, 13, 16.7 or 22.4 mM glucose in presence of 10 μM TEPP-46, 10 μM GKa1 (PF PF-04967319) or 0.1% DMSO. To induce glucolipotoxicity in normal donors, islet re-aggregates were incubated for 72 h under control or glucolipotoxic conditions (1% fatty acid free BSA alone or conjugated with 1mM of 2:1 sodium oleate/sodium palmitate and 20 mM glucose), which were removed and replaced with DMEM as described above for the acute study. Supernatants were evaluated by insulin ELISA (ALPCO).

PEPCK Activity Assay: PEPCK activity was measured according the protocol (Catalog # K359 Biovision). Simply described, 70-100 islets were homogenized with 200 μL cold PEPCK assay buffer provided in the kit for 10 min on ice, then centrifuged at 10,000 μg at 4°C for 10 min. Supernatants were then collected and protein concentration was measured. 50 μl of sample and 50 μL of reaction mix consisting of PEPCK assay buffer, PEPCK converter, PEPCK developer, PEPCK probe and PEPCK substrate mix (Catalog # K359 Biovision) were added to each well and the plate was read at an OD of 570 nm.

Immunoblotting Analysis: Tissues were homogenized in lysis buffer supplemented with protease and phosphatase inhibitor cocktails (Roche) for protein isolation. Proteins from homogenized liver and skeletal muscle tissue (30 μg of protein extracts) were separated by 4%–12% SDS-PAGE (Invitrogen) and then transferred to PVDF membranes (Millipore) using a semidry transfer cell (Bio-Rad) for 120 min. After blockade of nonspecific sites with 5% nonfat dry milk Tris-buffered saline and Tween 20 (10mM Tris, 100mM NaCl, and 0.1% Tween 20) solution, membranes were incubated overnight at 4°C with primary antibodies. Membranes were thoroughly washed, incubated with the appropriate secondary antibody

(Cell Signaling Technology) and immune complexes were detected using an enhanced luminol chemiluminescence system (ECL; Thermo Scientific) and exposed to photographic film. Signals on the immunoblot were quantified by optical densitometry.

200 - 250 islets were homogenized in ice-cold homogenization buffer with protease and phosphatase inhibitors (cOmplete MINI + PhosSTOP (Roche)). Proteins were detected by western blot analysis after separating 30–50 μg of total protein lysate on a 4 - 12% Tris-glycine gel (BioRad) and transferring to a polyvinylidene difluoride membrane (Immobilon-P 0.45 μm, Millipore). Goat anti-PEPCK-M (Abcam) and rabbit anti-B-actin (cell signaling) were used. Antibody information was provided in the Key Resources Table.

Quantitative PCR: Total RNA was isolated from islets using buffer RLT and was further purified with the RNeasy kit (QIAGEN). The abundance of transcripts was assessed by real-time PCR on an Applied Biosystems 7500 Fast Real-Time PCR System with a SYBR Green detection system (Bio-Rad). The primer sequences are provided in key resource table. To generate the principal component analysis and heatmap the counts obtained from RTqPCR data was log transformed and normalized with respect to mean of the control samples to get a normal distribution followed by standardization through z-score in addition to the normalized data. PCA was generated using prcomp package in R and displayed using ggplot. To generate the heatmap, the data was plotted in such a manner that the mean of PKa samples was sorted in descending order. The heatmap was plotted in Prism.

PK Activity Assay: The enzymatic assay of pyruvate kinase (EC 2.7.1.40) protocol from Sigma was adapted to a 96 well plate format, and modified using a 5 mM PEP in the presence of 3 μM FBP.

GK Protein Assay: The amount of glucokinase protein was determined according the protocol from RayBiotech Elisa kit #catalog EL-PRELIM

PDKdKO Mice: Mice lacking pyruvate dehydrogenase kinase 2 and 4 (double knock out; DKO), resulting in constitutively activated PDH, were kindly provided by Dr. Robert A. Harris.

ASO Animal Study: The liver tissues from rats treated with insulin receptor anti-oligonucleotide (ASO) and control ASO were generous gift and the method was described previously (Vatner et al., 2015).

Liver Enzyme ALT, AST and Blood Gases Measurement: Liver enzymes aspartate transaminase (AST), alanine transaminase (ALT), and blood gasses (pH, bicarbonate, or pCO_2) were measured at Yale diabetic research center core.

Mass Spectroscopy

Preparation of Red Blood Cells: Blood were sampled from jugular venous catheter and immediately centrifuged 13,000 rpm for 30 s. Plasma was removed and RBCs were frozen in liquid nitrogen and stored at −80°C freezer until use. RBC samples were suspended in ice cold Quench buffer (150 μl) and quickly vortexed for 30 s followed by 6 subsequent vortex

cycles (Quench buffer: 20% Methanol, 0.1% formic acid, 3 mM NaF, 1mM phenylalanine, 100mm EDTA). Samples were then transferred to the lyophilizer. After 24 h lyophilizing, samples were suspended with water and mixed thoroughly for LC/MS/MS measurement.

LC-MS/MS and GC/MS Analysis: Plasma PK activator concentrations were determined by mass spectrometry using a SCIEX 5500 QTRAP equipped with a SelexION for differential mobility separation (DMS). Plasma samples were injected onto a Hypercarb column (3 μm particle size, 4.6x100mm, Thermo Fisher Scientific) at a flow rate of 0.4 mL/min. Plasma samples were eluted with a combination of aqueous (A: 15mM ammonium formate and 10μM EDTA) and organic mobile phase (B: 60% acetonitrile, 35% isopropanol and 15mM ammonium formate) according to the following gradient: t = 0 min, B = 0%; t = 0.5 min, B = 0%, t = 1 min, B = 40%; t = 1.5 min, B = 40%; t = 2 min, B = 0%; t = 6 min, B = 0%. Metabolite detection was based on multiple reaction monitoring (MRM) in negative mode using the following source parameters: CUR: 30, CAD: high, IS: ±1500, TEM: 625, GS1: 50 and GS2: 55.

Q1	Q3	t	ID	DP	EP	CE	CXP
373	373	10	PKa NIH 373/373	80	7	8	18
467	467	200	PKa2 Agios 467/467	−30	−8	−10	−20
467	403	200	PKa2 Agios 467/403	−30	−8	−50	−20

***In Vivo* Hepatic Metabolism—**Plasma glucose was derivatized and M+0 to M+7 isotopologues were measured in duplicate by GC/MS as previously described and corrected for background using samples from uninfused rats and natural abundance as well as the small fraction of M+5 glucose in the tracer (Perry et al., 2015). MIDA analysis was performed by removing the M+6 glucose signal when calculating the glucose isotopomers using the following relationships to calculate the enrichment of the triose phosphates assuming DHAP and G3P to be in isotopic equilibrium and diluted by unlabeled glycerol, glycogen, and plasma glucose:

$$\mathrm{P0} = \mathrm{TrioseM+0} = (\mathrm{Glucose+0})^{1/2} \quad \text{(Equation 1)}$$

$$\mathrm{P1} = \mathrm{TrioseM+1} = \mathrm{GlucoseM+1}/(2^{*}\mathrm{TrioseM+0}) \quad \text{(Equation 2)}$$

$$\mathrm{P2} = \mathrm{TrioseM+2} = (\mathrm{GlucoseM+2} - \mathrm{TrioseM+1}^{2})/(2^{*}\mathrm{TrioseM+0}) \quad \text{(Equation 3)}$$

$$\mathrm{P3} = \mathrm{TrioseM+3} = (\mathrm{GlucoseM+3} - \mathrm{TrioseM+2}^{*}\mathrm{TrioseM+1}^{*}2) / (2^{*}\mathrm{TrioseM+0}) \quad \text{(Equation 4)}$$

Assumptions

- The relationships are based on the presence of isotopic steady state (or pseudo-steady state) which was confirmed in Figures 5G–5L.
- Because of low enrichments, there are no combinations of PC + PDH labeling (only species below considered).
- PC, PCK, and PK are functionally irreversible
- PC and PCK account for the majority of anaplerosis and cataplerosis, respectively
- V_{CS} is approximately equivalent to V_{SDH}
- At steady state, the carbon label in OAA cycle via PC is diluted by unlabeled carbon in exchange with the TCA cycle (e.g., glutamate ↔ αKG) by a constant amount empirically measured as *k.*
- Fumarase fully racemizes OAA and Mal
- MIDA of glucose to obtain the triose phosphate isotopologues approximates the PEP isotopologues.
- Plasma lactate is in rapid equilibrium with hepatic lactate.

Mass Balance: $V_{PC} = V_{PCK} = V_{GNG} + V_{PK} = V_{LDH} + V_{PK}$ (Figure 6C)

$V_{PC} + V_{SDH} = V_{CS} + V_{PCK}$

Isotopomer Naming: (* = ^{13}C, ° = ^{12}C, labeled left to right sequentially)

Malate/OAA

M3a = ***°; M3b = °***

M2a = **°°; M2b = °°**, M2c = °**°

Pyruvate, PEP, Lactate

L3,P3,Py3 = ***

P2a,Py2a = °**

P2b,Py2b = **°

Isotopomer Relationships: Isotopologues

P2 = P2a + P2b

M3 = M3a + M3b

M2 = M2a + M2b + M2c

Racemization

M3a = M3b	(***° ↔ °***)
M2a = M2b	(**°° ↔ °°**)

Precursor → Product: PCK

M3a = P3	(***° → ***)
M3b + M2c = P2a	(°*** + °***° → °**)
M2a = P2b	(**°° → **°)

PC

Pyr3 → 0.5(M3a + M3b)	(*** → 0.5(***° + °***))
Pyr2a → M2c	(°** → °**°)
Pyr2b → 0.5(M2a +M2b)	(**° → 0.5(**°° + °°**))

LDH

Lac3 → Pyr3

PK

PEP3 → Pyr3

PEP2a → Pyr2a

PEP2b → Pyr2b

TCA

M3a + M3b = (M2a + M2b)	(***° + °*** → *k*(**°° + °°**))
M2c = 0.5*k*(M2a + M2B)	(°**° → 0.5*k*(**°° + °°**))

Definitions of Variables: $A = V_{LDH}/V_{PCK}$

$B = V_{PK}/V_{PCK}$

A = 1-B

$D = V_{PCK}/(V_{CS} + V_{PCK})$

$E = V_{CS}/(V_{CS}+V_{PCK})$

D = 1-E

Isotope Balance: (Solved at isotopic steady state: δx/δt = 0)

$\delta P_3/\delta t$

$$\begin{aligned} &V_{LDH}(L_3/2) + V_{PK}(P_3/2) = (V_{PCK} + V_{CS})P_3 \\ &V_{LDH}/(V_{PCK} + V_{CS})(L_3/2) + V_{PK}/(V_{PCK} + V_{CS})(P_3/2) = P_3 \\ &A^*D(L_3/2) + B^*D(P_3/2) = P_3 \text{ (substitute)} \end{aligned} \quad \text{(Equation 5)}$$

$\delta P_{2a}/\delta t$

$$\begin{aligned} &V_{LDH}(L_3/2) + V_{PK}(P_3/2) + V_{PK}(P_3) = (V_{CS} + V_{PCK})(P_{2A}) \\ &A^*D(L_3/2) + B^*D(P_3/2) + B^*D(P_3) = P_{2A}(\text{substitute}) \\ &A^*D(L_3/2) + B^*D(P_3/2) = P_{2A} - B^*D(P_3) \end{aligned} \quad \text{(Equation 6)}$$

$\delta P_{2b}/\delta_t$

$$\begin{aligned} &[V_{LDH}(V_{CS}/V_{PCK} + V_{CS})]k(L_3/2) + [V_{PK}(V_{CS}/V_{PCK} + V_{CS})]k(P_3/2) \\ &= (V_{CS}+V_{PCK})(P_{2B}) \\ &[ADEk](L_3/2) + [BDEk](P_3/2) = P_{2B} \\ &(AD)(L_3/2) + (BD)(P_3/2) = P_{2B}/Ek \end{aligned} \quad \text{(Equation 7)}$$

Combine Equations 5 and 6

$$\begin{aligned} &P_3 = P_{2A} - B^*D(P_3) \\ &P_3 + B^*D(P_3) = P_{2A} \end{aligned} \quad \text{(Equation 8)}$$

Combine Equations 5 and 7

$$(Ek)P_3 = P_{2b} \quad \text{(Equation 9)}$$

(Substitute $P_2 = P_{2A} + P_{2B}$)

$$P_3 + B^*D(P_3) + (Ek)P_3 = P_2 \quad \text{(Equation 10)}$$

(Rearrange Equation 5)

$$\begin{aligned} &A^*D(L_3/2) + B^*D(P_3/2) = P_3 \\ &A^*D(L_3) + B^*D(P_3) = 2P_3 \\ &(1 - B)(L_3) + B^*D(P_3) = 2P_3(\text{substitute}) \end{aligned}$$

(Rearrange and solve for B*D)

$$B^{*}D = (2P_3 - L_3D)/(P_3 - L_3) \quad \text{(Equation 11)}$$

(Substitute Equation 11 into Equation 10)

$$P_3 + (2P_3 - L_3D)/(P_3 - L_3)(P_3) + (Ek)P_3 = P_2$$

(Solve for E)

$$V_{CS}/(V_{CS} + V_{PCK}) = E = [k(P_2/P_3 - 1)(P_3 - L_3) - 2P_3 + L_3]/P_3 \quad \text{(Equation 12)}$$

$$V_{PCK}/(V_{CS} + V_{PCK}) = D = 1 - E \quad \text{(Equation 13)}$$

$$V_{PK}/V_{PCK} = B = (2P_3 - L_3D)/(D(P_3 - L_3)) \quad \text{(Equation 14)}$$

$$V_{LDH}/V_{PCK} = A = 1 - B \quad \text{(Equation 15)}$$

Relative Mitochondrial Fluxes

$$V_{PCK}/V_{CS} = D/E \quad \text{(Equation 16)}$$

$$V_{PK}/V_{LDH} = B/A \quad \text{(Equation 17)}$$

$$V_{PK}/V_{CS} = BE \quad \text{(Equation 18)}$$

$$V_{LDH}/V_{CS} = AE \quad \text{(Equation 19)}$$

Absolute Hepatic Fluxes: Given that V_{CS} could be different in control and treated groups, it is helpful to have absolute rates of metabolic flux for side by side comparisons. With a few previously evaluated assumptions (Perry et al., 2017), it is possible to estimate the absolute rates of hepatic metabolism by relating the directly measured rate of EGP to the relative rates of hepatic metabolism production. Since kidneys consume as much glucose as they produce (Perry et al., 2014), the net rates of hepatic metabolism are tied by mass balance to the directly measured endogenous glucose production rate (R_a):

$$R_a = 2 * V_{GNG} * \phi_{PEP \rightarrow Glucose}, \quad \text{(Equation 20)}$$

where the fractional contribution of PEP to glucose ($\phi_{PEP \rightarrow Glucose}$) estimates the contribution of mitochondrial gluconeogenesis contributes to the EGP. The higher order isotopologues of glucose (M+4 and M+5) measured versus predicted by reverse MIDA

estimates the amount of M0 triose and hexose diluting the trioses originating in the mitochondria. These differences were below the level of error and not different between the groups. Similarly, rates of the glucose to alanine and glutamine cycles were not different (Figure 5I). Therefore, rather than introducing an unmeasured correction, $\phi_{PEP \rightarrow Glucose} = 1$ was used such that $R_a \approx 2*V_{GNG}$ that over-estimates the mitochondrial gluconeogenesis equally for both groups. By mass balance, $V_{LDH} = V_{GNG}$ individual hepatic flux rates can be derived through a combination of Equation 16 with Equations 12, 13, 14, and 15.

$$V_{GNG} = R_a/2 \quad \text{(Equation 21)}$$

$$V_{CS} = (R_a/2)/A^*E \quad \text{(Equation 22)}$$

$$V_{PK} = (R_a/2)^*(B/A) \quad \text{(Equation 23)}$$

$$V_{PC} = V_{GNG} + V_{PK} \quad \text{(Equation 24)}$$

QUANTIFICATION AND STATISTICAL ANALYSIS

Data Representation and Statistical Analysis—Data are displayed as bar graphs of at least three independent experiments and it include mean and SEM. Average ± SEM is represented.

Statistical significance was calculated by Student's t test and a one-way ANOVA with Tukey's post-test. All p values and n are reported in the figure legends. Results are considered significant when $p < 0.05$. Tracer analyses were performed on an LC/MS/MS in a blinded fashion. Data demonstrated and were analyzed as having a normal distribution unless otherwise stated. Mice and rats were randomly assigned to groups using sample sizes based on power calculations to demonstrate a 20% difference between groups based on prior experience. Exclusions were applied only if animals did not regain 95% post-surgical weight, catheters or infusions failed, or animals showed signs of infection or stress during the course of the experiment (~1 – 2 out of 10 samples based on these criteria).

Supplementary Material

Refer to Web version on PubMed Central for supplementary material.

ACKNOWLEDGMENTS

We thank Dr. Robert A. Harris and Yasmeen Rahimi for providing mice lacking PDK 2 and 4 (PDK double knockout; PDKDKO) and Pfizer for providing reagents. R.G.K. gratefully acknowledges the NIH/NIDDK (R01DK092606, R01DK110181, and K08DK080142), CTSA (UL1RR-0024139), and DRC (P30DK045735), as well as an investigator-initiated Sponsored Research Agreement from Agios Pharmaceuticals to Yale supporting this work. This work was supported in part by a Monash-Yale Strategic Grant Program in Metabolism to R. Stark and R.G.K. (MDO17PW01). R. Stark was supported by a National Health and Medical Research Council of Australia Early Career Fellowship. Z.B.A. was supported by a National Health and Medical Research Council of Australia Senior Research Fellowship (APP1154974). M.J.M. gratefully acknowledges support from the American

Diabetes Association (1–16-IBS-212), the NIH/NIDDK (K01DK101683 and R01DK113103), the NIH/NIA (R21AG050135 and R01AG062328), the Wisconsin Partnership Program, and the Central Society for Clinical and Translational Research. C.T. acknowledges the support of the Division of Preclinical Innovation, National Center for Advancing Translational Sciences.

REFERENCES

Akhmedov D, De Marchi U, Wollheim CB, and Wiederkehr A (2012). Pyruvate dehydrogenase E1α phosphorylation is induced by glucose but does not control metabolism-secretion coupling in INS-1E clonal β-cells. Biochim. Biophys. Acta 1823, 1815–1824. [PubMed: 22809973]

Alves TC, Pongratz RL, Zhao X, Yarborough O, Sereda S, Shirihai O, Cline GW, Mason G, and Kibbey RG (2015). Integrated, step-wise, mass-isotopomeric flux analysis of the TCA cycle. Cell Metab. 22, 936–947. [PubMed: 26411341]

Anastasiou D, Yu Y, Israelsen WJ, Jiang J-K, Boxer MB, Hong BS, Tempel W, Dimov S, Shen M, Jha A, et al. (2012). Pyruvate kinase M2 activators promote tetramer formation and suppress tumorigenesis. Nat. Chem. Biol 8, 839–847. [PubMed: 22922757]

Boxer MB, Jiang JK, Vander Heiden MG, Shen M, Skoumbourdis AP, Southall N, Veith H, Leister W, Austin CP, Park HW, et al. (2010). Evaluation of substituted N,N′-diarylsulfonamides as activators of the tumor cell specific M2 isoform of pyruvate kinase. J. Med. Chem 53, 1048–1055. [PubMed: 20017496]

Cline GW, Lepine RL, Papas KK, Kibbey RG, and Shulman GI (2004). 13C NMR isotopomer analysis of anaplerotic pathways in INS-1 cells. J. Biol. Chem 279, 44370–44375. [PubMed: 15304488]

De Ceuninck F, Kargar C, Ilic C, Caliez A, Rolin JO, Umbdenstock T, Vinson C, Combettes M, de Fanti B, Harley E, et al. (2013). Small molecule glucokinase activators disturb lipid homeostasis and induce fatty liver in rodents: a warning for therapeutic applications in humans. Br. J. Pharmacol 168, 339–353. [PubMed: 22925001]

Dechiara TM, Poueymirou WT, Auerbach W, Frendewey D, Yancopoulos GD, and Valenzuela DM (2009). VelociMouse: fully ES cell-derived F0-generation mice obtained from the injection of ES cells into eight-cell-stage embryos. Methods Mol. Biol 530, 311–324. [PubMed: 19266341]

Efanova IB, Zaitsev SV, Zhivotovsky B, Köhler M, Efendić S, Orrenius S, and Berggren PO (1998). Glucose and tolbutamide induce apoptosis in pancreatic beta-cells. A process dependent on intracellular Ca2+ concentration. J. Biol. Chem 273, 33501–33507. [PubMed: 9837930]

Erion DM, Lapworth A, Amor PA, Bai G, Vera NB, Clark RW, Yan Q, Zhu Y, Ross TT, Purkal J, et al. (2014). The hepatoselective glucokinase activator PF-04991532 ameliorates hyperglycemia without causing hepatic steatosis in diabetic rats. PLoS One 9, e97139. [PubMed: 24858947]

Ferdaoussi M, Dai X, Jensen MV, Wang R, Peterson BS, Huang C, Ilkayeva O, Smith N, Miller N, Hajmrle C, et al. (2015). Isocitrate-to-SENP1 signaling amplifies insulin secretion and rescues dysfunctional β cells. J. Clin. Invest 125, 3847–3860. [PubMed: 26389676]

Gassaway BM, Cardone RL, Padyana AK, Petersen MC, Judd ET, Hayes S, Tong S, Barber KW, Apostolidi M, Abulizi A, et al. (2019). Distinct hepatic PKA and CDK signaling pathways control activity independent pyruvate kinase phosphorylation and hepatic glucose production. Cell Rep. 29, 3394–3404.e9. [PubMed: 31825824]

Girousse A, Tavernier G, Valle C, Moro C, Mejhert N, Dinel AL, Houssier M, Roussel B, Besse-Patin A, Combes M, et al. (2013). Partial inhibition of adipose tissue lipolysis improves glucose metabolism and insulin sensitivity without alteration of fat mass. PLoS Biol. 11, e1001485. [PubMed: 23431266]

Grace RF, Rose C, Layton DM, Galacteros F, Barcellini W, Morton DH, van Beers EJ, Yaish H, Ravindranath Y, Kuo KHM, et al. (2019). Safety and efficacy of mitapivat in pyruvate kinase deficiency. N. Engl. J. Med 381, 933–944. [PubMed: 31483964]

Harris RA, and Fenton AW (2019). A critical review of the role of M2PYK in the Warburg effect. Biochim Biophys Acta Rev Cancer 1871, 225–239. [PubMed: 30708038]

Iwakura T, Fujimoto S, Kagimoto S, Inada A, Kubota A, Someya Y, Ihara Y, Yamada Y, and Seino Y (2000). Sustained enhancement of Ca(2+) influx by glibenclamide induces apoptosis in RINm5F cells. Biochem. Biophys. Res. Commun 271, 422–428. [PubMed: 10799313]

James MO, Jahn SC, Zhong G, Smeltz MG, Hu Z, and Stacpoole PW (2017). Therapeutic applications of dichloroacetate and the role of glutathione transferase zeta-1. Pharmacol. Ther 170, 166–180. [PubMed: 27771434]

Jensen MV, Joseph JW, Ronnebaum SM, Burgess SC, Sherry AD, and Newgard CB (2008). Metabolic cycling in control of glucose-stimulated insulin secretion. Am. J. Physiol. Endocrinol. Metab 295, E1287–E1297. [PubMed: 18728221]

Jeoung NH, Rahimi Y, Wu P, Lee WN, and Harris RA (2012). Fasting induces ketoacidosis and hypothermia in PDHK2/PDHK4-double-knockout mice. Biochem. J 443, 829–839. [PubMed: 22360721]

Jesinkey SR, Madiraju AK, Alves TC, Yarborough OH, Cardone RL, Zhao X, Parsaei Y, Nasiri AR, Butrico G, Liu X, et al. (2019). Mitochondrial GTP links nutrient sensing to β cell health, mitochondrial morphology, and insulin secretion independent of OxPhos. Cell Rep. 28, 759–772.e10. [PubMed: 31315053]

Jiang JK, Boxer MB, Vander Heiden MG, Shen M, Skoumbourdis AP, Southall N, Veith H, Leister W, Austin CP, Park HW, et al. (2010). Evaluation of thieno[3,2-b]pyrrole[3,2-d]pyridazinones as activators of the tumor cell specific M2 isoform of pyruvate kinase. Bioorg. Med. Chem. Lett 20, 3387–3393. [PubMed: 20451379]

Kibbey RG, Pongratz RL, Romanelli AJ, Wollheim CB, Cline GW, and Shulman GI (2007). Mitochondrial GTP regulates glucose-stimulated insulin secretion. Cell Metab. 5, 253–264. [PubMed: 17403370]

Kibbey RG, Choi CS, Lee HY, Cabrera O, Pongratz RL, Zhao X, Birkenfeld AL, Li C, Berggren PO, Stanley C, and Shulman GI (2014). Mitochondrial GTP insensitivity contributes to hypoglycemia in hyperinsulinemia hyperammonemia by inhibiting glucagon release. Diabetes 63, 4218–4229. [PubMed: 25024374]

Lewandowski SL, Cardone RL, Foster HR, Ho T, Potapenko E, Poudel C, VanDeusen HR, Sdao SM, Alves TC, Zhao X, et al. (2020). Pyruvate kinase controls signal strength in the insulin secretory pathway. Cell Metab. 32, this issue. ■■■–■■■.

Lu D, Mulder H, Zhao P, Burgess SC, Jensen MV, Kamzolova S, Newgard CB, and Sherry AD (2002). 13C NMR isotopomer analysis reveals a connection between pyruvate cycling and glucose-stimulated insulin secretion (GSIS). Proc. Natl. Acad. Sci. USA 99, 2708–2713. [PubMed: 11880625]

MacDonald MJ, and Chang CM (1985a). Do pancreatic islets contain significant amounts of phosphoenolpyruvate carboxykinase or ferroactivator activity? Diabetes 34, 246–250. [PubMed: 3882492]

MacDonald MJ, and Chang CM (1985b). Pancreatic islets contain the M2 isoenzyme of pyruvate kinase. Its phosphorylation has no effect on enzyme activity. Mol. Cell. Biochem 68, 115–120. [PubMed: 3908905]

MacDonald MJ, and Fahien LA (1988). Glyceraldehyde phosphate and methyl esters of succinic acid. Two “new” potent insulin secretagogues. Diabetes 37, 997–999. [PubMed: 3290012]

MacDonald MJ, McKenzie DI, Walker TM, and Kaysen JH (1992). Lack of glyconeogenesis in pancreatic islets: expression of gluconeogenic enzyme genes in islets. Horm. Metab. Res 24, 158–160. [PubMed: 1601389]

MacDonald MJ, Fahien LA, Brown LJ, Hasan NM, Buss JD, and Kendrick MA (2005). Perspective: emerging evidence for signaling roles of mitochondrial anaplerotic products in insulin secretion. Am. J. Physiol. Endocrinol. Metab 288, E1–E15. [PubMed: 15585595]

Madiraju AK, Erion DM, Rahimi Y, Zhang XM, Braddock DT, Albright RA, Prigaro BJ, Wood JL, Bhanot S, MacDonald MJ, et al. (2014). Metformin suppresses gluconeogenesis by inhibiting mitochondrial glycerophosphate dehydrogenase. Nature 510, 542–546. [PubMed: 24847880]

Madiraju AK, Qiu Y, Perry RJ, Rahimi Y, Zhang XM, Zhang D, Camporez JG, Cline GW, Butrico GM, Kemp BE, et al. (2018). Metformin inhibits gluconeogenesis via a redox-dependent mechanism in vivo. Nat. Med 24, 1384–1394. [PubMed: 30038219]

Malaisse-Lagae F, Bakkali Nadi A, and Malaisse WJ (1994). Insulinotropic response to enterally administered succinic and glutamic acid methyl esters. Arch. Int. Pharmacodyn. Ther 328, 235–242. [PubMed: 7710308]

Matschinsky FM, and Ellerman JE (1968). Metabolism of glucose in the islets of Langerhans. J. Biol. Chem 243, 2730–2736. [PubMed: 4870741]

Miyanaga O, Nagano M, and Cottam GL (1982). Effect of insulin on liver pyruvate kinase in vivo and in vitro. J. Biol. Chem 257, 10617–10623. [PubMed: 7050117]

Newgard CB, Lu D, Jensen MV, Schissler J, Boucher A, Burgess S, and Sherry AD (2002). Stimulus/secretion coupling factors in glucose-stimulated insulin secretion: insights gained from a multidisciplinary approach. Diabetes 51 (Suppl 3), S389–S393. [PubMed: 12475781]

Olofsson CS, Göpel SO, Barg S, Galvanovskis J, Ma X, Salehi A, Rorsman P, and Eliasson L (2002). Fast insulin secretion reflects exocytosis of docked granules in mouse pancreatic B-cells. Pflugers Arch. 444, 43–51. [PubMed: 11976915]

Palomino-Schätzlein M, Lamas-Domingo R, Ciudin A, Gutiérrez-Carcedo P, Marés R, Aparicio-Gómez C, Hernández C, Simó R, and Herance JR (2020). A translational in vivo and in vitro metabolomic study reveals altered metabolic pathways in red blood cells of type 2 diabetes. J. Clin. Med 9,1619.

Parks WC, and Drake RL (1982). Insulin mediates the stimulation of pyruvate kinase by a dual mechanism. Biochem. J 208, 333–337. [PubMed: 6760859]

Perry RJ, Zhang XM, Zhang D, Kumashiro N, Camporez JP, Cline GW, Rothman DL, and Shulman GI (2014). Leptin reverses diabetes by suppression of the hypothalamic-pituitary-adrenal axis. Nat. Med 20, 759–763. [PubMed: 24929951]

Perry RJ, Camporez JG, Kursawe R, Titchenell PM, Zhang D, Perry CJ, Jurczak MJ, Abudukadier A, Han MS, Zhang XM, et al. (2015). Hepatic acetyl CoA links adipose tissue inflammation to hepatic insulin resistance and type 2 diabetes. Cell 160, 745–758. [PubMed: 25662011]

Perry RJ, Peng L, Cline GW, Butrico GM, Wang Y, Zhang XM, Rothman DL, Petersen KF, and Shulman GI (2017). Non-invasive assessment of hepatic mitochondrial metabolism by positional isotopomer NMR tracer analysis (PINTA). Nat. Commun 8, 798. [PubMed: 28986525]

Petersen KF, Dufour S, Befroy D, Garcia R, and Shulman GI (2004). Impaired mitochondrial activity in the insulin-resistant offspring of patients with type 2 diabetes. N. Engl. J. Med 350, 664–671. [PubMed: 14960743]

Pongratz RL, Kibbey RG, Shulman GI, and Cline GW (2007). Cytosolic and mitochondrial malic enzyme isoforms differentially control insulin secretion. J. Biol. Chem 282, 200–207. [PubMed: 17102138]

Prentki M, Matschinsky FM, and Madiraju SR (2013). Metabolic signaling in fuel-induced insulin secretion. Cell Metab. 18, 162–185. [PubMed: 23791483]

Samuel VT, Petersen KF, and Shulman GI (2010). Lipid-induced insulin resistance: unravelling the mechanism. Lancet 375, 2267–2277. [PubMed: 20609972]

Schuit F, Van Lommel L, Granvik M, Goyvaerts L, de Faudeur G, Schraenen A, and Lemaire K (2012). β-cell-specific gene repression: a mechanism to protect against inappropriate or maladjusted insulin secretion? Diabetes 61 , 969–975. [PubMed: 22517647]

Shalev A (2014). Minireview: Thioredoxin-interacting protein: regulation and function in the pancreatic β-cell. Mol. Endocrinol 28, 1211–1220. [PubMed: 24911120]

Sharma G, Wu CY, Wynn RM, Gui W, Malloy CR, Sherry AD, Chuang DT, and Khemtong C (2019). Real-time hyperpolarized ^{13}C magnetic resonance detects increased pyruvate oxidation in pyruvate dehydrogenase kinase 2/4-double knockout mouse livers. Sci. Rep 9, 16480. [PubMed: 31712597]

Shi JH, Lu JY, Chen HY, Wei CC, Xu X, Li H, Bai Q, Xia FZ, Lam SM, Zhang H, et al. (2020). Liver ChREBP protects against fructose-induced glycogenic hepatotoxicity by regulating L-type pyruvate kinase. Diabetes 69, 591–602. [PubMed: 31974143]

Staal GE, Rijksen G, Vlug AM, Vromen-van den Bos B, Akkerman JW, Gorter G, Dierick J, and Petermans M (1982). Extreme deficiency of L-type pyruvate kinase with moderate clinical expression. Clin. Chim. Acta 118, 241–253. [PubMed: 7055983]

Stark R, Pasquel F, Turcu A, Pongratz RL, Roden M, Cline GW, Shulman GI, and Kibbey RG (2009). Phosphoenolpyruvate cycling via mitochondrial phosphoenolpyruvate carboxykinase links anaplerosis and mitochondrial GTP with insulin secretion. J. Biol. Chem 284, 26578–26590. [PubMed: 19635791]

Titchenell PM, Lazar MA, and Birnbaum MJ (2017). Unraveling the regulation of hepatic metabolism by insulin. Trends Endocrinol. Metab 28, 497–505. [PubMed: 28416361]

Valenzuela DM, Murphy AJ, Frendewey D, Gale NW, Economides AN, Auerbach W, Poueymirou WT, Adams NC, Rojas J, Yasenchak J, et al. (2003). High-throughput engineering of the mouse genome coupled with high-resolution expression analysis. Nat. Biotechnol 21, 652–659. [PubMed: 12730667]

Vatner DF, Majumdar SK, Kumashiro N, Petersen MC, Rahimi Y, Gattu AK, Bears M, Camporez JP, Cline GW, Jurczak MJ, et al. (2015). Insulin-independent regulation of hepatic triglyceride synthesis by fatty acids. Proc. Natl. Acad. Sci. USA 112, 1143–1148. [PubMed: 25564660]

Wang H, Chu W, Das SK, Ren Q, Hasstedt SJ, and Elbein SC (2002). Liver pyruvate kinase polymorphisms are associated with type 2 diabetes in northern European Caucasians. Diabetes 51, 2861–2865. [PubMed: 12196482]

Wu CY, Tso SC, Chuang JL, Gui WJ, Lou M, Sharma G, Khemtong C, Qi X, Wynn RM, and Chuang DT (2018). Targeting hepatic pyruvate dehydrogenase kinases restores insulin signaling and mitigates ChREBP-mediated lipogenesis in diet-induced obese mice. Mol. Metab 12, 12–24. [PubMed: 29656110]

Yang H, Merica E, Chen Y, Cohen M, Goldwater R, Kosinski PA, Kung C, Yuan ZJ, Silverman L, Goldwasser M, et al. (2019). Phase 1 single- and multiple-ascending-dose randomized studies of the safety, pharmacokinetics, and pharmacodynamics of AG-348, a first-in-class allosteric activator of pyruvate kinase R, in healthy volunteers. Clin. Pharmacol. Drug Dev 8, 246–259. [PubMed: 30091852]

Yu C, Chen Y, Cline GW, Zhang D, Zong H, Wang Y, Bergeron R, Kim JK, Cushman SW, Cooney GJ, et al. (2002). Mechanism by which fatty acids inhibit insulin activation of insulin receptor substrate-1 (IRS-1)-associated phosphatidylinositol 3-kinase activity in muscle. J. Biol. Chem 277, 50230–50236. [PubMed: 12006582]

Zawalich WS, Zawalich KC, Cline G, Shulman G, and Rasmussen H (1993). Comparative effects of monomethylsuccinate and glucose on insulin secretion from perifused rat islets. Diabetes 42, 843–850. [PubMed: 8388341]

Highlights

- Pyruvate kinase activators (PKa) amplify insulin release in preclinical T2DM models
- PKa amplify insulin release via the phosphoenolpyruvate cycle *in vivo*
- PKa acutely short-circuit gluconeogenesis and accelerate red blood cell glycolysis
- PKa improve insulin sensitivity, steatosis, and dyslipidemia in obese rats

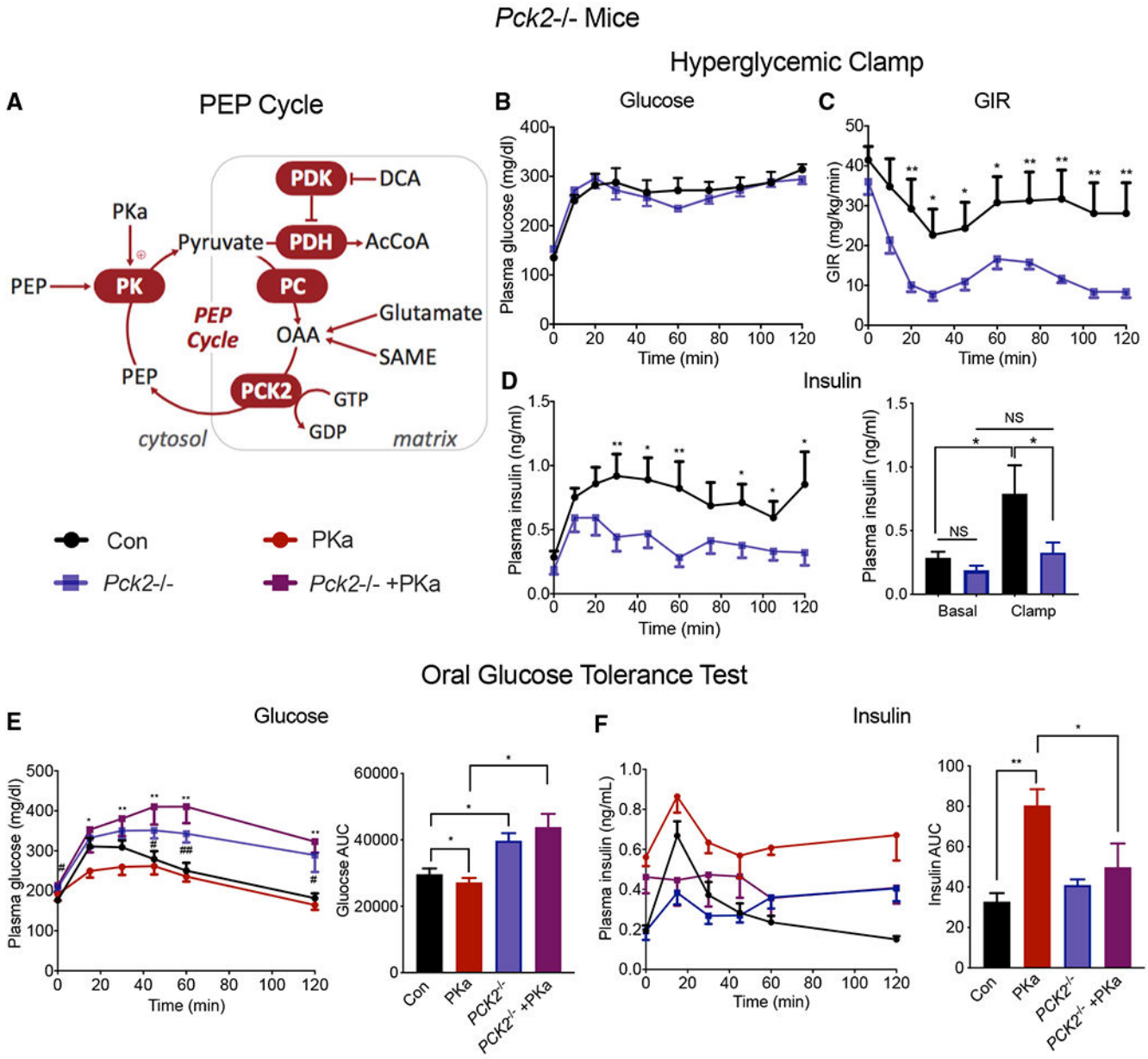

Figure 1. *Pck2*$^{-/-}$ Is Required for Normal and PK Activator Amplified GSIS *In Vivo*

(A) Schematic overview of strategies for assessing the OxPhos-independent mitochondrial GTP (mtGTP)-dependent phosphoenolpyruvate (PEP) cycle. Oxidation of pyruvate by pyruvate dehydrogenase (PDH) is inhibited by phosphorylation by PDH kinase (PDK) that is in turn inhibited by dichloroacetic acid (DCA) or by knockout. Anaplerotic synthesis of oxaloacetic acid (OAA) is from pyruvate carboxylase (PC) or via metabolism of succinic acid methyl ester (SAME) or glutamate. OAA cataplerosis of OAA to generate PEP is through the GTP-dependent PCK2 reaction. Cytosolic and mitochondrial PEP are hydrolyzed via pyruvate kinase (PK) that is allosterically enhanced with PK activators. (B and C) Plasma glucose concentrations (B) and glucose infusion rate (GIR) (C) in overnight fasted mice during a hyperglycemic clamp.

(D) Insulin (left) during same clamp study and (right) before clamp (basal), and average plasma insulin levels of clamp (105–120 min).
(E) Glucose homeostasis in overnight fasted WT (black), WT + PKa (red), *Pck2*$^{-/-}$ (blue), and *Pck2*$^{-/-}$ + PKa (purple) following an OGTT 1 h after PKa (50 mg/kg) injection. Area under the curve (AUC) plasma glucose following an OGTT.
(F) Stimulated and AUC insulin from the OGTT in (E) in mice fasted overnight.
Data are represented as mean ± SEM (OGTT, n = 7–8 per group; hyperglycemic clamp, n = 8 per group). Statistical comparisons (*$p < 0.05$, **$p < 0.01$; NS, not significant) made by Student's t test.

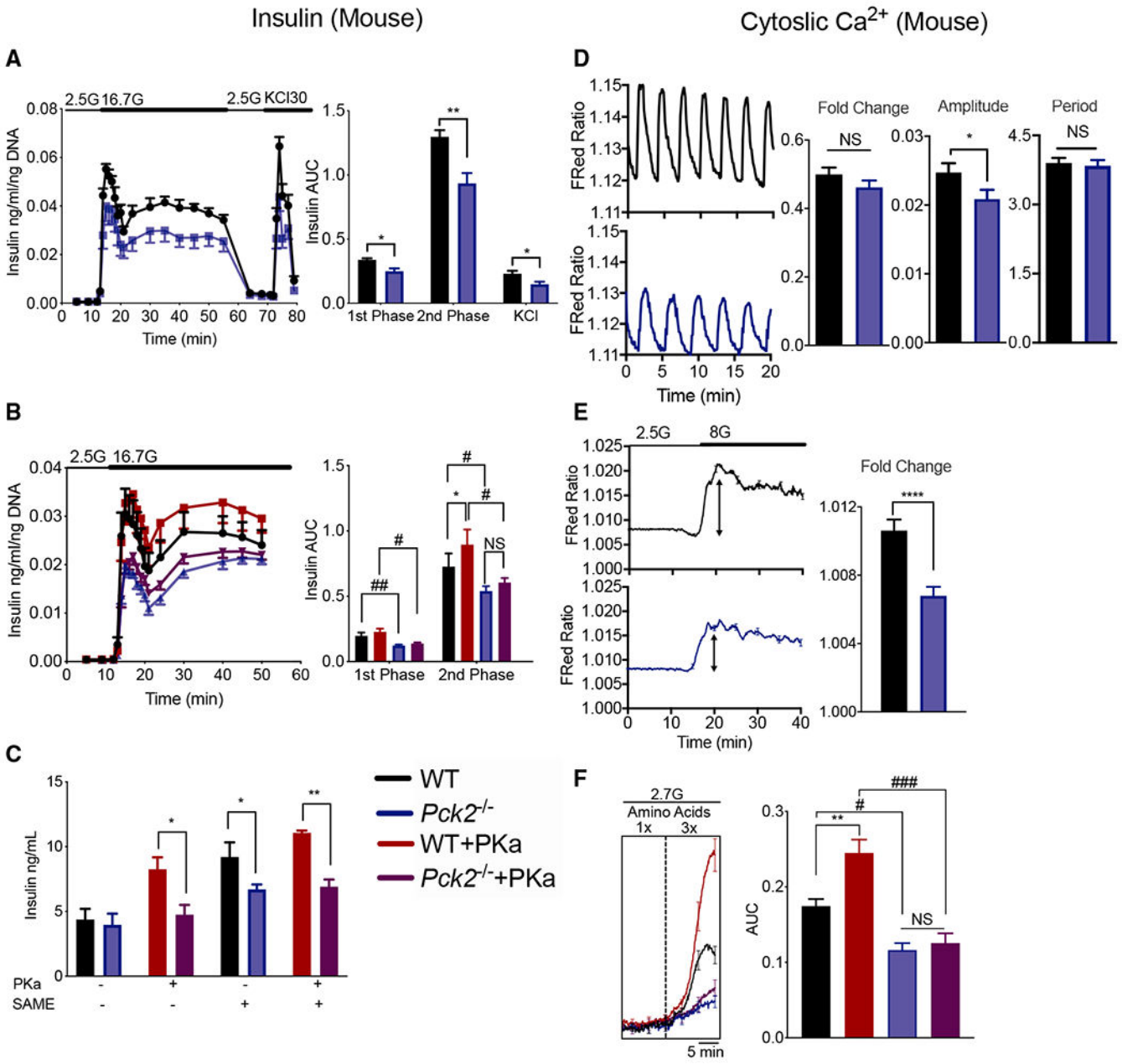

Figure 2. PCK2 Is Required for the Anaplerosis and PK-Dependent Secretory Response

(A) Phasic insulin secretion during perifusion from 2.5 to 16.7 mM glucose (G) of islets followed by 30 mM KCI stimulation from control (wild type; WT) and *Pck2*$^{-/-}$ (n = 4).

(B) Phasic insulin secretion during perifusion from 2.5 to 16.7 mM glucose of islets from control (WT) and *Pck2*$^{-/-}$ with or without treatment with 10 μM PKa (Tepp46) (n = 4).

(C) Insulin secretion from isolated, dispersed, and reaggregated islets ± 10 μM PKa ± 10 mM SAME (n = 4).

(D and E) Cytosolic calcium recordings, in the presence of indicated glucose and amino acids concentrations from control (black) and *Pck2*$^{-/-}$ (blue) islets.

(D) Detrended calcium traces, fraction of time spent in the active phase (plateau fraction), average calcium amplitude, and period of time from islets held at 8 mM glucose in physiologic amino acids (n = 3 mice/group).
(E) Ca^{2+} response following an acute increase of glucose in islets from WT and *Pck2*$^{-/-}$ mice.
(F) Cytosolic Ca^{2+} in response to one (1×) and three times physiologic (3×) amino acids at 2.7 mM glucose ± 10 μM TEPP46 (PKa) (n = 8). Scale bar, 5 min.
Data are represented as mean ± SEM. Statistical comparisons made by Student's t test and two-way ANOVA (*p < 0.05, **p < 0.01, ***p < 0.001, #p < 0.05, ##p < 0.01).

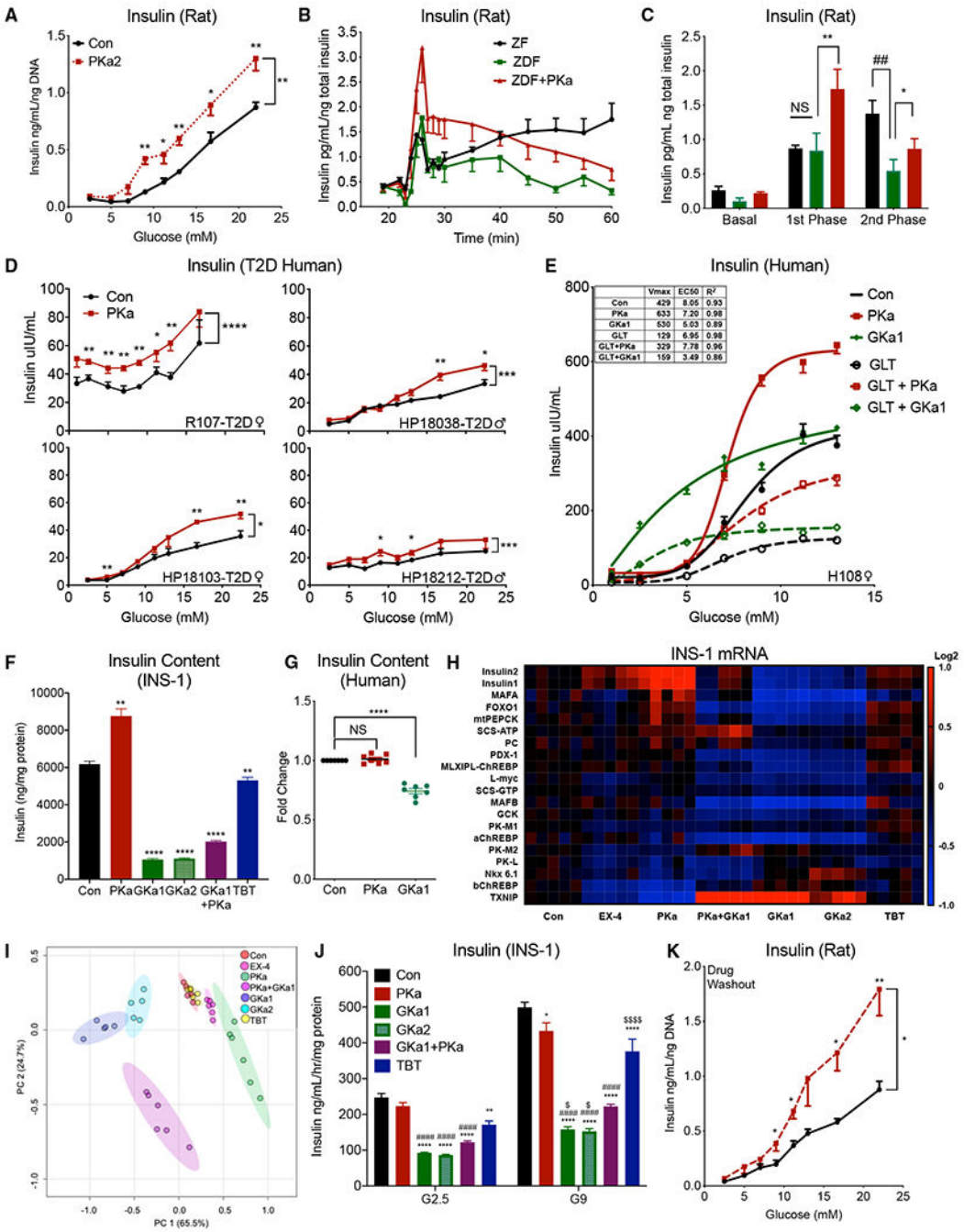

Figure 3. PK Activation Improves Insulin Secretion in Rat and Human Islet Models of Insulin Resistance and Type 2 Diabetes

(A) Insulin response to glucose concentration in re-aggregated islets from 4-week HFD-fed rats with twice daily peanut butter vehicle without (black) or with 25 mg/kg PKa2 (red) (n = 4) but without exposure to drug for 16 h.

(B and C) Phasic insulin secretion from perifused islets (2.5–16.7 mM glucose) from regular chow (ZF, black) and high-fatfed (ZDF) Zucker rats without (green) and with (red) 10 μM PKa (n = 4).

(D) Insulin response to glucose concentration in islet reaggregates from four type 2 diabetes islet donors (R107, HP18038, HP18103, and HP18212) treated with 10 μM PKa.
(E) Insulin response to glucose concentration from healthy human reaggregated islets treated for 72 h with BSA control (closed) versus glucolipotoxic (GLT, 20 mM glucose and 1 mM 2:1 oleate:palmitate) (open) conditions without (black circles) or with 10 μM PKa (red squares) or 10 μM GKa (green diamonds).
(F) Insulin content from INS-1 cells treated with 10 μM PKa, 10 μM GKa1, 100 nM GKa2, the combination of PKa and GKa1, or 100 μM TBT for 72 h.
(G) Insulin content from 7 healthy human donors treated for 72 h in culture with 10 μM PKa or 10 μM GKa1.
(H and I) Transcriptional profiling of INS-1 cells treated with 10 μM GKa1, 100 nM GKa2, 10 μM PKa, 10 nM Ex-4, or 100 μM TBT for 72 h.
(J) INS cells were treated for 72 h with 10 μM GKa1, 100 μM GKa2, 10 μM PKa, and 100 mM TBT, then drug was washed out prior to performing GSIS assays.
(K) Islets were isolated from combined 4-week HFD- and PKa2-treated rats and GSIS was performed.
Data are represented as mean ± SEM. Statistical comparisons made by Student'sttest and two-way ANOVA (*with versus without PKa; $^{\#}$ZF versus ZDF or control versus GLT; $^{*,\#}p < 0.05$, $^{**,\#\#}p < 0.01$).

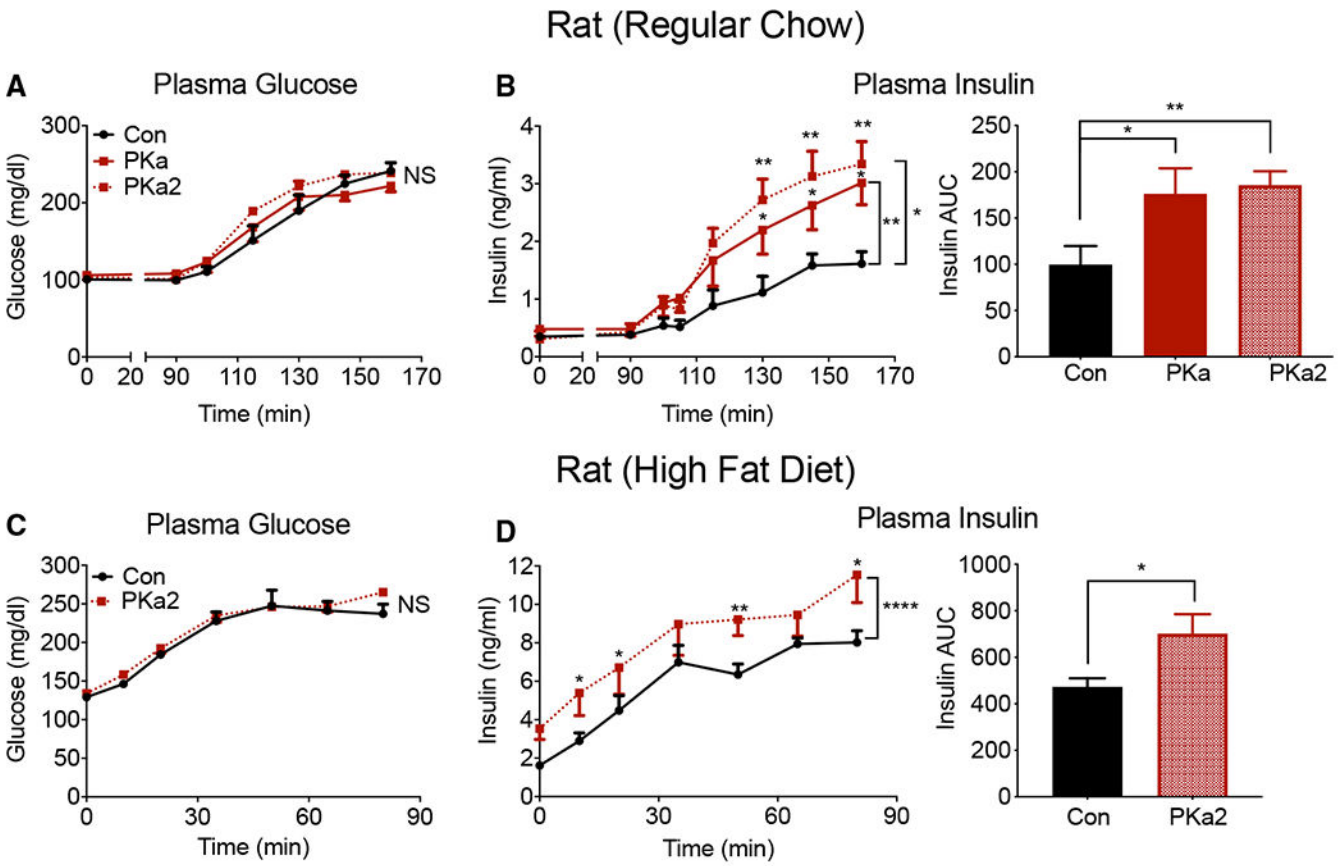

Figure 4. PK Activation Improves GSIS in Regular Chow and HFD-Fed Rats

(A and B) Plasma glucose (A) and plasma insulin (B), and insulin AUC after primed-continuous intravenous infusion (t = 0) followed by hyperglycemic ramp (t = 90–160 min) of PKa1 and PKa2 versus vehicle in overnight fasted regular chow-fed rats (n = 6–7 per group).

(C and D) Plasma glucose (C) and plasma insulin (D), and insulin AUC in 4-week HFD-fed rats with twice daily administration of peanut butter vehicle without (black) or with PKa2 (red), then subjected to a hyperglycemic ramp after an overnight fast without subsequent drug treatment (n = 6–7 per group).

Statistical comparisons made by Student's t test and two-way ANOVA (*p < 0.05, **p < 0.01).

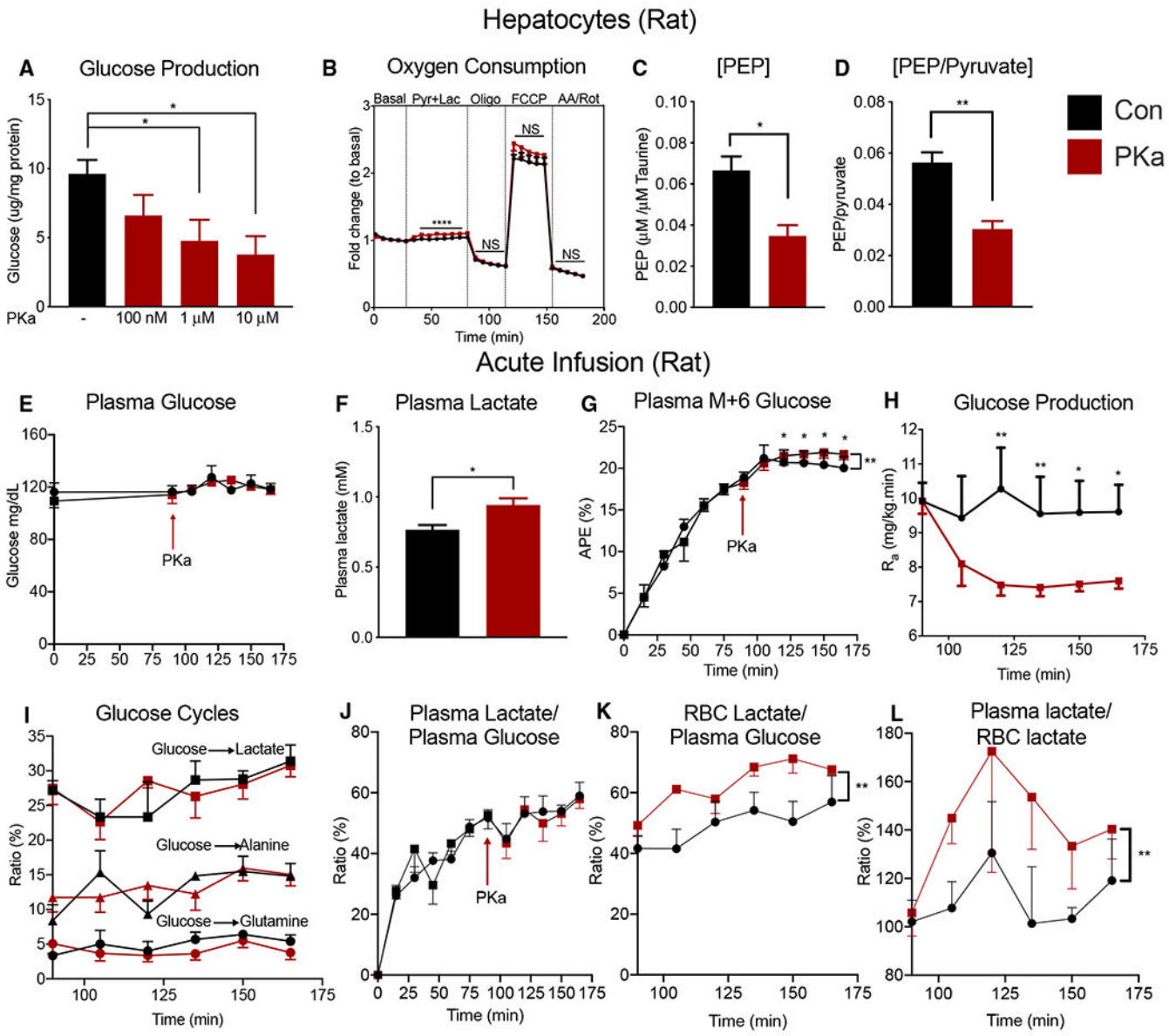

Figure 5. PK Activation Short-Circuits Gluconeogenesis and Increases RBC Glucose Turnover

(A) Glucose production from isolated hepatocytes treated with the indicated concentration of PKa (n = 6).

(B) Oxygen consumption rates of hepatocytes treated with 10 μM PKa under basal conditions followed by pyruvate (1 mM):lactate(9 mM) substrate addition, 5 μM oligomycin, 10 μM FCCP, and 5 μM rotenone (n = 6).

(C and D) Liquid chromatography-tandem mass spectrometry (LC-MS/MS) measured absolute PEP concentration from isolated hepatocytes treated with or without 10 μM PKa and ratio of PEP to pyruvate calculated (n = 6).

(E) Plasma glucose during acute PKa infusion.

(F) Plasma lactate concentration of acutely PKa-infused overnight fasted chow-fed rats.

(G) Plasma glucose M+6 enrichment of overnight fasted regular chow-fed rats infused with PKa and [U $^{13}C_6$]-D-glucose tracer (n = 6–7).
(H) Endogenous glucose production rate from overnight fasted chow-fed Sprague-Dawley rats acutely infused with PKa.
(I) The enrichments of M+2 glutamine, M+3 alanine, and M+3 lactate by their circulating precursor (M+6 glucose).
(J) Ratio of plasma lactate enrichment (M+3) to total plasma glucose enrichment (M+6) in rats treated with or without PKa.
(K) Ratio of red blood cell (RBC) lactate (M+3) to plasma glucose (M+6) in rats treated with and without PKa.
(L) Ratio of RBC lactate enrichment (M+3) to plasma lactate enrichment.
Data are represented as mean ± SEM. Statistical comparisons made by Student's t test and two-way ANOVA (*$p < 0.05$, **$p < 0.01$, ***$p < 0.001$) (n = 6–7) for all infusion studies.

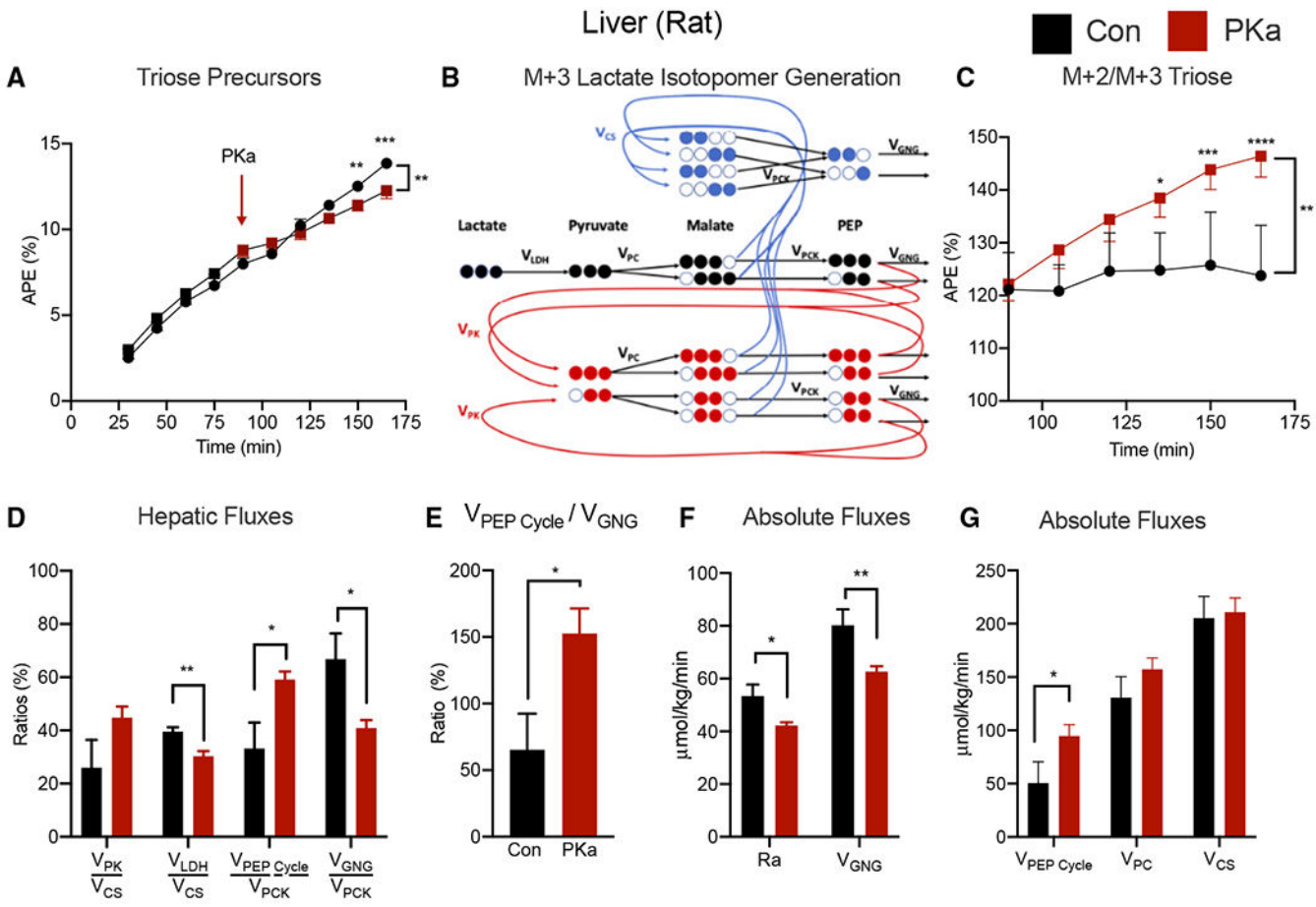

Figure 6. PK Activation Reduces EGP *In Vivo*

(A) Isotopologues of the mitochondrial-derived those precursors from gluconeogenic tissues deconvolved via a mass isotopomer distribution analysis (MIDA) of glucose isotopologues.

(B) Schematic for stable isotope interpretation: filled circles are ^{13}C and open circles are ^{12}C. M+3 lactate (black) enters the mitochondria, and gluconeogenic PEP isotopomers are generated as a function of the relative contributions of TCA cycling (blue), PEP cycling (red), and PC.

(C) M+2/M+3 those ratio increased following PKa administration.

(D and E) TCA cycle flux (V_{CS}), rates of net LDH metabolism (V_{LDH}), rates of PEP cycling ($V_{PEP\ Cycling}/V_{PCK}$), and mitochondrial gluconeogenic flux (V_{GNG}/V_{PCK}) are shown.

(F and G) Absolute *in vivo* rates of cycling and gluconeogenic fluxes were determined (n = 5).

Data are represented as mean ± SEM. Statistical comparisons made by Student's t test and two-way ANOVA (*p < 0.05, **p < 0.01, ***p < 0.001).

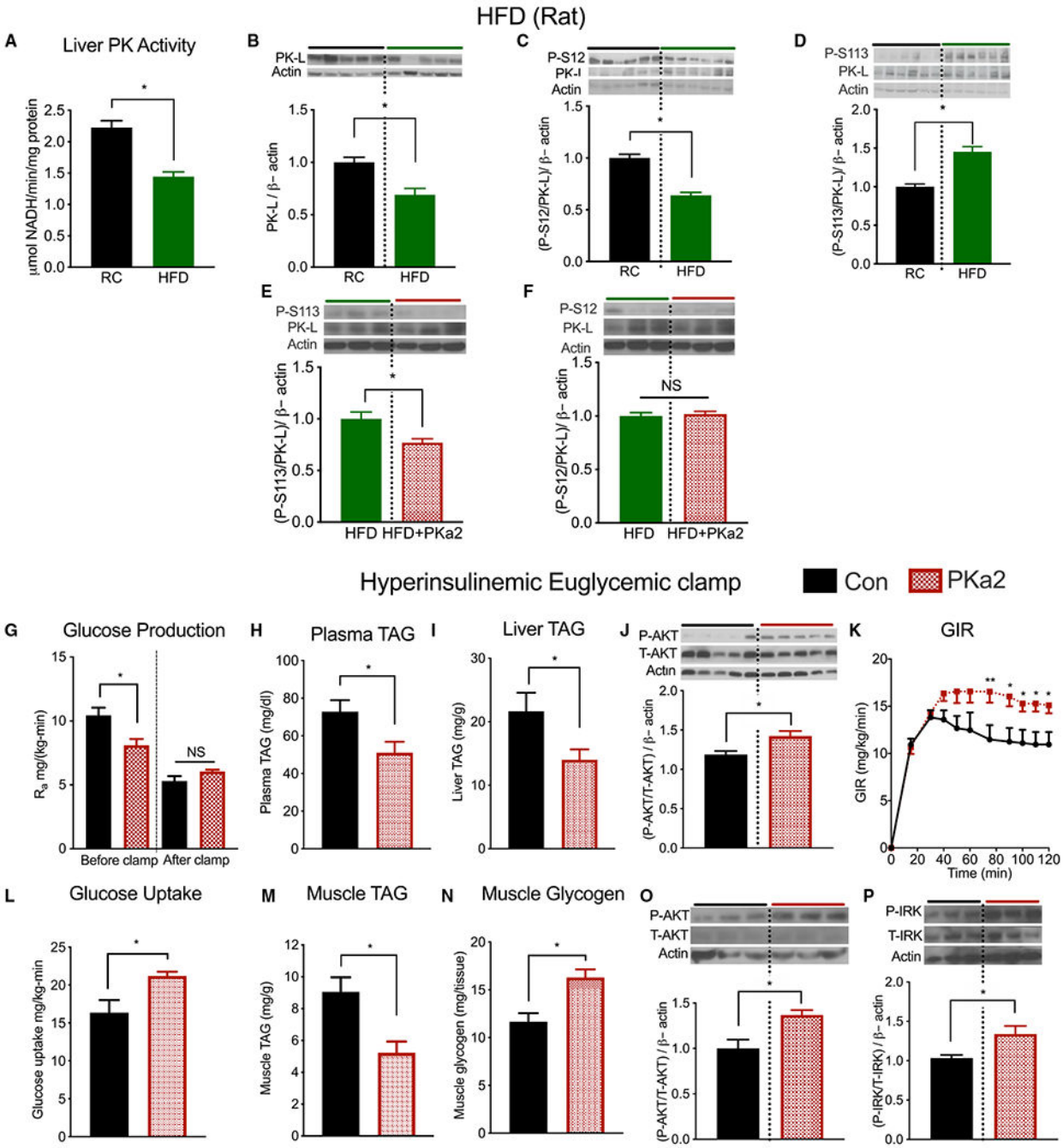

Figure 7. Chronic PKa during HFD Feeding Improves Insulin Sensitivity and Reduces Ectopic Fat

(A and B) Liver pyruvate kinase (PKL) activity and protein expression of HFD-fed and regular chow (RC)-fed rats.

(C) PKL phosphorylation (S12) in liver tissue of HFD-fed and RC-fed mice.

(D) PKL phosphorylation at (S113) in liver tissue of HFD-fed and RC-fed mice.

(E) PKL phosphorylation (S113) in liver tissue of control (HFD) versus chronic PKa2-treated rats.

(F) PKL phosphorylation (S12) in liver tissue of control (HFD) versus chronic PKa2-treated rats.

(G) Endogenous glucose production.

(H and I) Plasma TAG content of 4-week chronic PKa2-treated HFD-fed rats (H) and liver TAG content (I) (n = 8).

(J) Liver AKT phosphorylation after 4-week PKa2 treatment of HFD-fed rat (n = 5).

(K) GIR during the hyperinsulinemic-euglycemic clamp.

(L) Insulin stimulated whole-body glucose uptake.

(M and N) Muscle TAG (M) and glycogen (N) content.

(O and P) Muscle AKT and insulin receptor kinase (IRK) tyrosine phosphorylation after 4-week PKa2 treatment of HFD-fed rat (n = 6); representative data shown. n = 4, fatty acid turnover. n = 7–8, hyperinsulinemic clamp.

Data are represented as mean ± SEM. Data analyzed by two-tailed unpaired Student’s t test and two-way ANOVA.

KEY RESOURCES TABLE

REAGENT or RESOURCE	SOURCE	IDENTIFIER
Antibodies		
Goat anti-PEPCK-M	Abcam	40843
PKL pS113 (A/G purified)	Covance-Custom Antibody	N/A
PKL pS12 (A/G purified)	Covance-Custom Antibody	N/A
PKL	Protein tech	AB_10918271
Phospho-AKT (ser 473)	Cell signaling	#9271
Total AKT	Cell signaling	#9272
Phospho-insulin receptor beta	Cell signaling	#3023S
Insulin receptor beta	Cell signaling	#3020S
Rabbit anti-beta-actin	Cell signaling	4970
Bacterial and Virus Strains		
Biological Samples		
Human islets	University of Alberta Diabetes Institute	NA
Human islets	University of Chicago Diabetes Research and Training Center	NA
Human islets	Prodo Laboratories Inc	NA
Chemicals, Peptides, and Recombinant Proteins		
DMEM-Base Cell culture media	Sigma Aldrich	D5030
RPMI 1640 Cell culture media	Sigma Aldrich	R8758
Quantitect reverse transcriptase	Qiagen	205311
SYBR PCR reagent	BioRad	1708880
CMRL culture media	GIBCO	NA
Complete mini EDTA-free protease inhibitor cocktail (Roche)	Sigma Aldrich	11836170001
PKa2	Agios pharmaceutical INC	AGI-17540
PKa (TEPP-46)	National Institute of Health	NA
GKa2	MK-0941	
GKa1	PF-04967319	
Glycogen	Sigma	10901393001
Glucosidase	Sigma	G5003
High Fat Diet	Dyets	#112245
Critical Commercial Assays		
Micro BCA protein assay kit	Thermo Fisher Scientific	23235
Rat High Range ELISA	ALPCO	80-INSRTH-E10
Mouse Ultrasensitive ELISA	ALPCO	80-INSMSU-E01
RNeasy Mini Kit	Qiagen	74106
DNeasy Blood & Tissue Kit	Qiagen	69504
PEPCK Activity Assay	Biovision	K359
HR Series NEFA-HR(2) Color Reagent A	Wako	999-34691

REAGENT or RESOURCE	SOURCE	IDENTIFIER
HR series NEFA-HR(2) solvent A	Wako	995-34791
HR Series NEFA-HR(2) Color Reagent B	Wako	991-34891
HR series NEFA-HR(2) solvent B	WAKO	993-35191
NEFA standard solution	WAKO	276-76491
TRIGLYCERIDE-SL	SEKISUI	236-99
GlUCOSE-SL	SEKISUI	235-60
Human Insulin ELISA	ALPCO	80-INSHU-E10
Deposited Data		
Experimental Models: Cell Lines		
Clonal INS-1 832/13 cell line over-expressing the human insulin gene (INS-1)	C.B. Newgard (Duke University School of Medicine)	N/A
Rat insulinoma cells (INS-1)	NA	NA
Experimental Models: Organisms/Strains		
Denoted C57BL/6NTac-Pck2$^{tm1\ (KOMP)Vlcg}$, project ID VG13655	University of California Davis Knockout Mouse Project repository	NA
ZDF (obese)	Charles river	370
ZDF (lean)	Charles river	371
Oligonucleotides		
Genotyping primer PCK2 FWD:	acttgctttaaaaaacctcccaca	N/A
Genotyping primer PCK2 REV:	gaggcggaaattggttctgcaatgg	N/A
Insulin2 FWD:	cagtgccaaggtctgaaggt	N/A
Insulin2 REV:	cagcacctttgtggttctca	N/A
Insulin1 FWD:	ctgcccaggcttttgtcaa	N/A
Insulin1 REV:	tccccacacaccaggtacaga	N/A
MafA FWD:	tccaggctggtgcgcgaaag	N/A
MafA REV:	gcaagcccactcaggagccg	N/A
FOXO1 FWD:	cacagtccaagcgctcaa	N/A
FOXO1 REV:	gtgaacaccatgcctcac	N/A
mtPEPCK (PCK2) FWD:	ttatgcacgatccctttgccatgc	N/A
mtPEPCK (PCK2) REV:	tccttcctttggtacgagcccaat	N/A
SCS-ATP FWD:	tgtggtacggttacaaggtaca	N/A
SCS-ATP REV:	acaaccattttagcagcttcat	N/A
PC FWD:	agatgcacttccatcccaag	N/A
PC REV:	ccttggtcacgtgaaccttt	N/A
Pdx1 FWD:	gacacatcaaaatctggttccaaa	N/A
Pdx1 REV:	tcccgctactacgtttcttatcttc	N/A
MLXIPL-CHREBP FWD:	tactgttccctgcctgctc	N/A
MLXIPL-CHREBP REV:	cttggaaaccttcaccagg	N/A
Lmyc FWD:	gaaggtgcatccgtaccact	N/A
Lmyc REV:	tctggggaatagccttgatg	N/A

REAGENT or RESOURCE	SOURCE	IDENTIFIER
SCS-GTP FWD:	gaggaagaggaaaaggtgtctt	N/A
SCS-GTP REV:	tctagaaatatccagggcttca	N/A
MafB FWD:	gaagcccgcgaggcatat	N/A
MafB REV:	ggccctggcactcacaaa	N/A
GCK FWD:	cttggtccaattgaggagga	N/A
GCK REV:	cagtggagcgtgaagacaaa	N/A
PKM1 FWD:	tggagagcatgatcaagaagc	N/A
PKM1 REV:	agggggtctgtggattgact	N/A
aChREBP FWD:	tgcatcgatcacaggtcatt	N/A
aChREBP REV:	aggctcaagcattcgaagag	N/A
PK-M2 FWD:	tggagagcatgatcaagaagc	N/A
PK-M2 REV:	cactgcagcacttgaaggag	N/A
PK-L FWD:	taagcaacgtagcagcatgg	N/A
PK-L REV:	cgatatccagaaggcagagg	N/A
NKx 6.1 FWD:	tcttctggcctggggtgatg	N/A
NKx 6.1 REV:	ggctgcgtgcttctttctcca	N/A
bChREBP FWD:	tctgcagatcgcgcggag	N/A
bChREBP REV:	cttgtcccggcatagcaac	N/A
TXNIP FWD:	cgagtcaaagccgtcaggat	N/A
TXNIP REV	ttcatagcgcaagtagtccaaggt	N/A
Recombinant DNA		
Software and Algorithms		
ImageJ software	(NIH; https://imagej.nih.gov/ij/)	N/A
El-MAVEN and Polly software	Elucidata	N/A
GraphPad Prism 7 software	GraphPad	N/A
Other		
Spectromax 384 Plus Spectrophotometer	Molecular Devices	
Analox GL5 Analyzer	Anolox InstrumentsLTD, UK	
Biorep Perifusion Instrument	Biorep Technologies	
Multiquant v2.1	Sciex	
SCIEX 5500 QTRAP equipped with a SelexION for differential mobility separation (DMS)	Sciex	
Hypercarb Column (3μm particle size, 4.6x100 mm)	Thermo Fisher Scientific	35003-104630
Hamamatsu ORCA-Flash4.0 V2 Digital CMOS camera	NA	NA
Nikon Elements and custom MATLAB software	NA	NA